Graphical Abstract

Synthesis

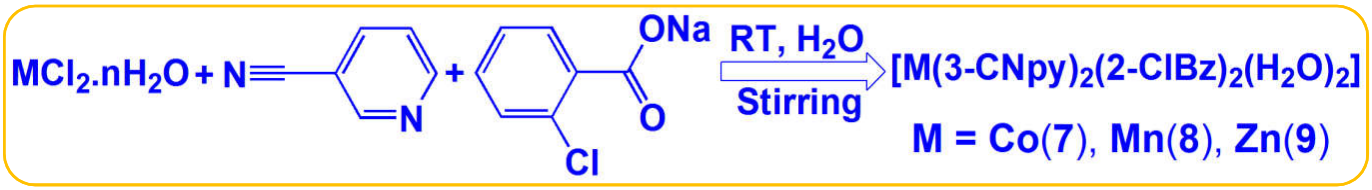

Molecular Structures

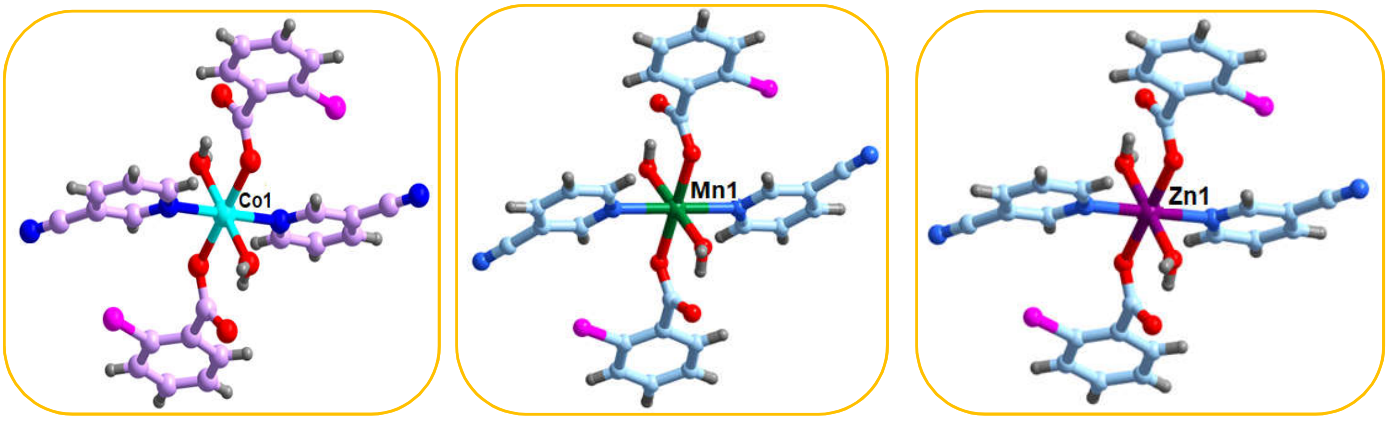

7 8 9

Self-Assembly

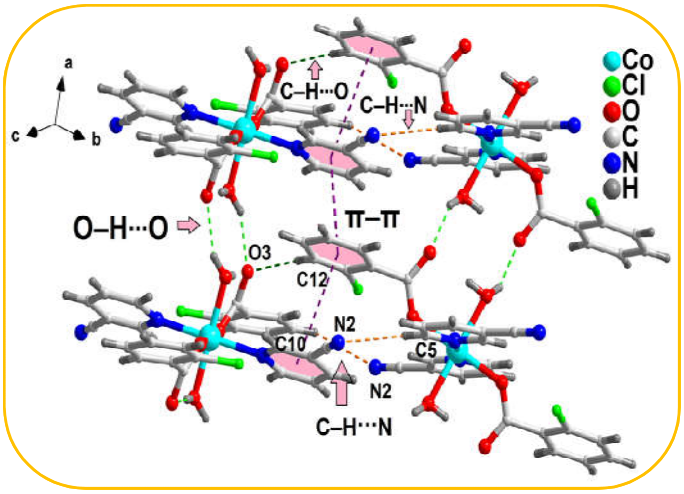

Theoretical Studies

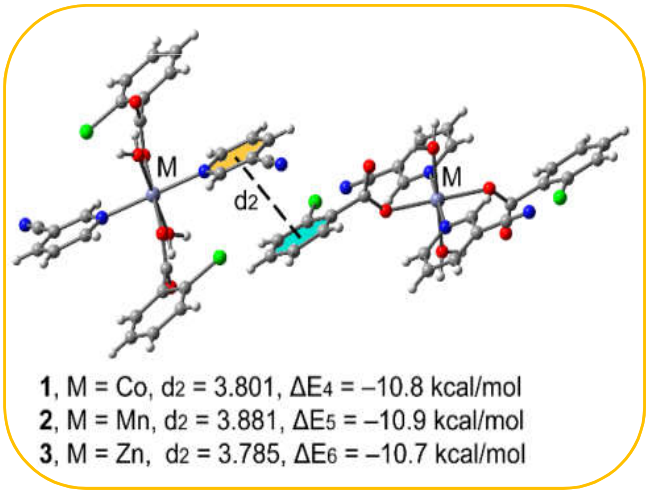

Apoptosis Assay

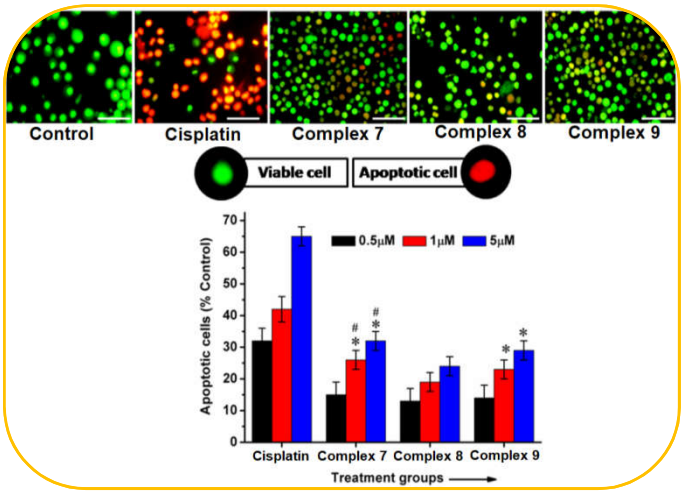

Docking

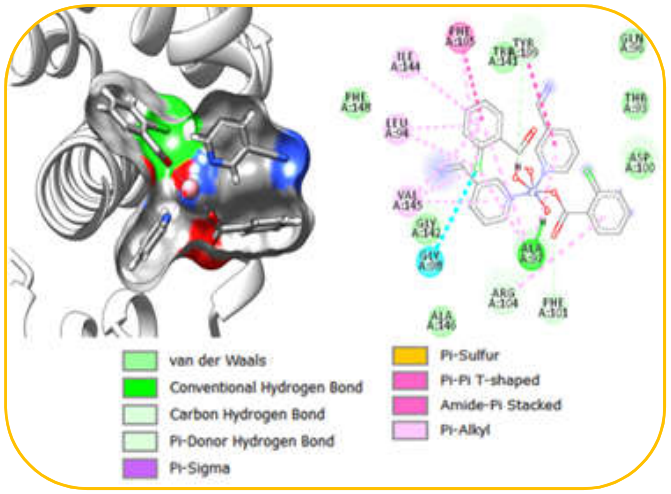

Chapter 4

Supramolecular Assemblies in Isostructural Coordination Compounds of Mn(II), Co(II) and Zn(II) Chlorobenzoates: Synthesis, Antiproliferative Evaluation and Theoretical Studies

4.1 INTRODUCTION

The design and construction of metal-organic networks has emerged as the field of current research interest due to their intriguing variety of structural topologies and various potential applications as functional materials.[1] The rational design and synthesis of the prospective metal-organic networks with the specific properties can be realized by careful selection of the organic/inorganic moieties as ligands that can explore interesting structures in the solid state.[2] The dynamic character of the metal-ligand bonds, nature and coordinating topologies of the ligands, metal-ligand ratio, different coordination geometries of the metal centers, nature of the counter ions and a variety of experimental conditions (such as the temperature, solvents and methods of crystallization) control the supramolecular assemblies in such networks.[3,4]

Carboxylate groups that can display a wide variety of coordination modes are used for designing mixed ligand complexes with interesting structures and topologies.[5] The structures of the ancillary ligands and reaction conditions have been shown to have profound effects on the binding mode of carboxylate moiety of substituted benzoates (2-chlorobenzoate, 4-chlorobenoate etc.) at the metal centers.[6] S. A. Adonin *et al*. have recently reported a coordination complex of Cu(II) involving 2-chlorobenzoate *viz*. $[Cu_2(2\text{-}ClBz)_4(acetone)_2]$ (where, 2-ClBz = 2-chlorobenzoate).[7] In the crystal structure, the binuclear complex fragments are reported to connect via Cl···Cl contacts. Moreover, properties of metal carboxylates and the coordination abilities of carboxylate ions can be varied to a large extent by using nitrogen donor ligands with appropriate

functionalization.[8] The applications of metal complexes derived from carboxylate ligand are diverse, which include material chemistry[9], medicine[10] and biology.[11] The synthesis of carboxylate-based coordination compounds has received considerable interest in fields of supramolecular chemistry and crystal engineering for their rich biochemistry with numerous biological activities such as antitumor, anticandida and antimicrobial.[12] Recently, D. Hegde and coworkers have successfully carried out *in vitro* anticancer evaluation of 2-chlorobenzoyl based transition metal complexes by MTT and apoptosis assay [acridine orange/ethidium bromide (AO/EB) staining method].[13]

The interpretation of the non-covalent interactions in coordination complexes that form the basis of highly specific molecular recognition, transport, and regulation mechanisms, lays the foundation for the interdisciplinary field of metallo-supramolecular assemblies.[14] The most dramatic changes in the properties of such molecules in the solid state has been triggered by non-covalent interactions involving π-stacking, anion–π, cation–π and C–H···π contacts due to their relative strength, directionality and ability to act synergically which provide the organizing force for the association of molecules.[15] Mono and polycarboxylate ligands have gained remarkable emphasis in metallo-supramolecular assemblies because of their bridging coordination behaviour, which results in the construction of desired one-, two- and three-dimensional simple or interpenetrated architectures.[16] Feng Su *et al*. have reported interesting magnetic properties of four isostructural 3D carboxylate coordination polymers $[M(H_2bpta)]_n$ [where, H_4bpta = 2,2′,4,4′-biphenyltetracarboxylic acid, M = Fe(II), Ni(II), Cu(II) and Zn(II)].[17] The synthesis and photoluminescence properties of two isostructural compounds *viz*. [M(HIMDC)(4,4′-bipyO)0.5(H_2O)] [where, H_3IMDC = 4, 5-imidazoledicarboxylate, 4,4′-bipyO = 4,4′-bipyridine-N,N′-dioxide, M = Co(II) and Zn(II)] have also been reported.[18] Q. Guan and his group have reported antimicrobial, antiproliferative and DNA binding properties of three novel transition metal isostructural complexes *viz*. $[ML_2(phen)]\cdot H_2O$ [where, M = Mn(II), Co(II), Zn(II); HL = 2-phenyl-4-selenazole carboxylic acid, phen = 1,10-phenanthroline].[19] The complexes induce significant cytotoxicity against human pancreatic (*PANC-28*) and hepatocarcinoma cell lines (*HuH7*).[19]

Experimental and theoretical evidences of interesting synergetic effects between anion–π and hydrogen bonding and between anion-π and π–π stacking contacts have

been reported; the interplay between these interactions can lead to strong cooperativity effects.[20] The mutual effects between non-covalent forces involving π-stacking, hydrogen bonding, halogen bonding and metal coordination can lead not only to electrostatic enhancement of interactions but also to remarkable cooperativity effects.[21] These effects are even more noticeable in systems where the nitrogen atom is forming part of the π-system of the rings.[22] In the extended supramolecular structures formed by building blocks involving aromatic ligands, such π-stacking interactions can contribute to self-assembly or molecular recognition processes.[23] These π–π interactions are important in large biological systems as well as relatively small molecules.[24] In order to achieve truly fruitful evidence as well as significance of such mutual effects, proper fusion of experimental and theoretical studies are of utmost importance.[25]

In the present chapter, we have discussed the synthesis and crystal structure of three isostructural Co(II), Mn(II) and Zn(II) coordination complexes of mixed N- and O-donor ligands *viz*. $[M(3\text{-CNpy})_2(2\text{-ClBz})_2(H_2O)_2]$ [M = Co(**7**), Mn(**8**) and Zn(**9**)] under mild conditions in purely aqueous medium. Apart from reporting the synthesis and crystal structure of the compounds, we also aim to study the weak non-covalent interactions that may govern the stability of the structures. We will also highlight the isostructurality aspect of the compounds **7**, **8** and **9** using Fábián & Kálmán approach. We also aim to establish theoretically the electrostatically enhanced π–π interactions that are observed in the complexes. We have used the molecular DFT, MEP surface and NCI plot index computational tools to evaluate energetically the strength of the π-stacked contacts and the effect of the metal on such interaction energies. We also aim to study the cytotoxicity, apoptosis inducing potential of the compounds in DL malignant cancer cells and *in silico* docking studies to find the binding affinity of the complexes **7**, **8** and **9** with BCL-2, an important apoptosis regulating protein in multiple cancer types. Further, we have also identified the important pharmacophore features that are responsible for structure activity relationship (SAR) of the complexes.

4.2 EXPERIMENTAL

4.2.1 Materials and methods

All reagents used in this work were obtained from commercial sources and used as received. The reactions were carried out in de-ionized water medium. Perkin Elmer

2400 Series II CHNS/O analyzer was used for elemental (C, H and N) analyses. KBr phase FT-IR spectra were recorded in a Brukar APEX II FT-IR spectrophotometer in the mid-IR region (4000 to 500 cm^{-1}). The diffuse-reflectance UV-Vis-NIR spectra were recorded using a Shimadzu UV-2600 spectrophotometer. Thermogravimetric studies were carried out under the flow of N_2 gas using a Mettler Toledo TGA/DSC1 STAR^e system at the heating rate of 10°C min^{-1}. The powder X-ray diffraction (PXRD) data were recorded using a XPERT-PRO X-ray powder diffractometer with Cu-Kα radiation. Room temperature magnetic susceptibility was measured at 300 K on a Sherwood Mark 1 Magnetic Susceptibility balance by Evans method.

4.2.2 Preparation of the complexes

4.2.2.1 Preparation of [Co(3-CNpy)$_2$(2-ClBz)$_2$(H$_2$O)$_2$] (7)

The compound **7** was prepared by the reaction of an aqueous solution of cobalt(II) chloride hexahydrate, $CoCl_2 \cdot 6H_2O$ (1.0 mmol, 0.238 g) with 3-cyanopyridine (2.0 mmol, 0.208 g) followed by the addition of sodium salt of 2-chlorobenzoic acid (2.0 mmol, 0.357 g) (**Scheme 4.1**). The reaction mixture was stirred at room temperature for two hours. The red precipitate so obtained was then filtered and the filtrate was left unperturbed in cooling conditions for crystallization. After about two weeks, block shaped, reddish single crystals of compound **7** suitable for X-ray analysis were obtained. The large crystals were filtered off, washed with small portion of water and dried at ambient temperature in air. Yield: 0.512 g (83%). Anal. calcd. for $C_{26}H_{20}Cl_2CoN_4O_6$ (Mw = 614.29): C, 50.83%; H, 3.28%; N, 9.12%. Found: C, 50.71%; H, 3.22%; N, 9.06%. IR spectral data (KBr disc, cm^{-1}): 3449(s), 2236(m), 1596(sh), 1409(s), 1048(s), 809(s), 762(s), 701(s), 646(s), 556(sh) [s, strong; m, medium; w, weak; br, broad; sh, shoulder]. μ_{eff} = 3.86 BM.

4.2.2.2 Preparation of [Mn(3-CNpy)$_2$(2-ClBz)$_2$(H$_2$O)$_2$] (8)

The synthesis of **8** is similar to that for **7** except for cobalt(II) chloride hexahydrate substituted by manganese(II) chloride tetrahydrate, $MnCl_2 \cdot 4H_2O$ (1.0 mmol, 0.198 g) (**Scheme 4.1**). The colourless compound so obtained was then filtered and the filtrate was left unperturbed for crystallization in cooling condition. After about two weeks, needle shaped, pale yellow single crystals of compound **8** suitable for X-ray

analysis were obtained. The large crystals were filtered off, washed with small portion of water and dried at ambient temperature in air. Yield: 0.455 g (74%). Anal. calcd. for $C_{26}H_{20}Cl_2MnN_4O_6$ (Mw = 610.30): C, 51.17%; H, 3.30%; N, 9.18%. Found: C, 51.11%; H, 3.19%; N, 9.07%. IR spectral data (KBr disc, cm^{-1}): 3456(s), 2236(m), 1596(sh), 1409(s), 1052(s), 809(s), 764(s), 701(s), 649(s), 553(sh) [s, strong; m, medium; w, weak; br, broad; sh, shoulder]. μ_{eff} = 5.81 BM.

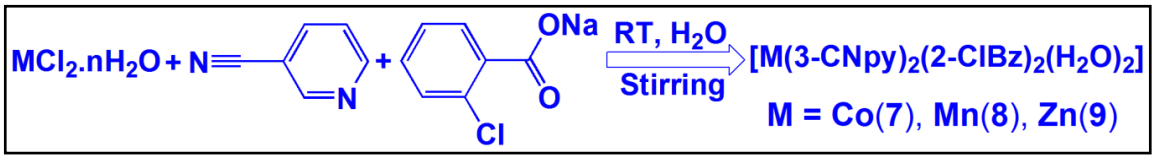

Scheme 4.1 Synthesis of compounds **7**, **8** and **9**.

4.2.2.3 Preparation of [Zn(3-CNpy)$_2$(2-ClBz)$_2$(H$_2$O)$_2$] (9)

Compound **9** was synthesized in a way similar to that for **7** except for cobalt(II) chloride hexahydrate substituted by zinc(II) chloride, $ZnCl_2$ (1.0 mmol, 0.136 g) (**Scheme 4.1**). The colourless compound so obtained was then filtered and the filtrate left unperturbed for crystallization. After about one week, block shaped, colourless single crystals of compound **9** suitable for X-ray analysis were obtained. The large crystals were filtered off, washed with small portion of water and dried at ambient temperature in air. Yield: 0.486 g (78%). Anal. calcd. for $C_{26}H_{20}Cl_2ZnN_4O_6$ (Mw = 620.73): C, 50.31%; H, 3.25%; N, 9.03%. Found: C, 50.25%; H, 3.13%; N, 8.95%. IR spectral data (KBr disc, cm^{-1}): 3476(s), 2236(m), 1596(sh), 1409(s), 1049(s), 809(s), 762(s), 701(s), 649(s), 555(sh) [s, strong; m, medium; w, weak; br, broad; sh, shoulder].

4.2.3 X-ray crystallographic procedures

Molecular and crystal structures of **7**, **8** and **9** were determined by single crystal X-ray diffraction techniques. Collection of X-ray crystallographic data and analyses of crystal structures have been done as detailed in Chapter 2. Crystal structures were solved by direct method (SHELXS) and refined by full matrix least squares techniques (SHELXL-2018/3) using the WinGX[26] platform available for personal computers. The hydrogen atoms in the compounds were located in difference Fourier maps and refined with isotropic atomic displacement parameters. The structural diagrams were drawn

with Diamond 3.2.[27] Data collection and refinement parameters for the complexes **7**, **8** and **9** are summarized in **Table 4.1**.

4.2.4 Theoretical methods

The geometry of one of the complex which is considered as a model of the three isostructural complexes was computed at the B3LYP-D/def2-TZVP level of theory using the crystallographic coordinates. For the calculations we have used the GAUSSIAN-09 program.[28] We have also used the Grimme's dispersion[29] correction, since it is adequate for the evaluation of non-covalent interactions. The basis set superposition error for the calculation of interaction energies has been corrected using the counterpoise method.[30] The molecular electrostatic potential (MEP) surfaces have been computed using the GAUSSIAN-09 program and the same level of theory. The NCI plot[31] isosurfaces have been used to characterize non-covalent interactions. They correspond to both favourable and unfavourable interactions, as differentiated by the sign of the second density Hessian eigen value and defined by the isosurface colour. The colour scheme is a red-yellow-green-blue scale with red for ρ^{+}_{cut} (repulsive) and blue for ρ^{-}_{cut} (attractive). The Gaussian-09 B3LYP-D/def2-TZVP level of theory wave function has been used to generate the NCI plot.

4.2.5 Cell line and drug preparation

The cytotoxicity and apoptosis inducing ability of the complexes **7**, **8** and **9** were evaluated *in vitro* condition (24 hours) using Dalton's lymphoma (DL) malignant cancer cell lines. The DL cells were cultured in RPMI-1640 supplemented with 10% FBS, gentamycin (20 mg/mL), streptomycin (100 mg/mL) and penicillin (100 IU) in a CO_2 incubator at 37°C with 5% CO_2; 80% confluent of exponentially growing cells were sub-cultured and used in the present study. The different doses (0, 0.01, 0.1, 0.5, 1, 5 and 10 μM) of the complexes **7**, **8** and **9** were prepared by dissolving in conditioned media (pH = 7.4).

4.2.6 MTT cell viability assay

The MTT cell viability assay is a colorimetric assay[32] and it is based on the ability of cellular oxidoreductase enzymes in presence of nicotinamide adenine

4.2.7 Crystal data

Table 4.1 Crystal and structure refinement data for **7**, **8** and **9**.

Parameters	**7**	**8**	**9**
Emprical formula	$C_{26}H_{20}Cl_2CoN_4O_6$	$C_{26}H_{20}Cl_2MnN_4O_6$	$C_{26}H_{20}Cl_2ZnN_4O_6$
Formulae weight	614.29	610.30	620.73
Temperature (K)	293(2)	293(2)	293(2)
Wavelength (Å)	0.71073	0.71073	0.71073
Crystal system	Monoclinic	Monoclinic	Monoclinic
Space group	$P2_1/c$	$P2_1/c$	$P2_1/c$
a/Å	7.0876(2)	7.207(5)	7.108(5)
b/Å	13.6906(4)	13.706(5)	13.623(5)
c/Å	14.1247(4)	14.195(5)	14.131(5)
α^o	90	90.000(5)	90.000(5)
β^o	101.261(2)	101.567(5)	101.725(5)
γ^o	90	90.000(5)	90.000(5)
Volume ($Å^3$)	1344.18(7)	1373.7(12)	1339.8(12)
Z	2	2	2
Calculated density (Mgm^{-3})	1.518	1.475	1.539
Absorption coefficient (mm^{-1})	0.885	0.722	1.164
F(000)	626	622	632
Crystal size (mm^3)	0.24 x 0.18 x 0.14	0.36 x 0.26 x 0.22	0.28 x 0.22 x 0.14
θ range for data collection (º)	2.09 to 28.08	2.09 to 29.94	2.93 to 29.86
Index ranges	–9<=h<=9, –17<=k<=18, –18<=l<=17	–10<=h<=10, –18<=k<=19, –19<=l<=18	–9<=h<=9,–19<=k<=13,–19<=l<=17
Reflections collected	23133	15185	14069
Refinement method	Full-matrix least-squares on F^2	Full-matrix least-squares on F^2	Full-matrix least-squares on F^2
Data / restraints / parameters	3194/0/178	3955/0/178	3762/0/178
Goodness-of-fit on F^2	1.047	1.039	1.062
Final *R* indices[$I>2\sigma(I)$] *R*1/ *wR*2	0.0294/0.0800	0.0356/0.0964	0.0290/0.0829
R indices (all data) *R*1/ *wR*2	0.0376/0.0842	0.0459/0.1034	0.0350/0.0862
Largest diff. peak and hole	0.299 and –0.311	0.434 and –0.414	0.419 and –0.343

$wR2 = \{\Sigma [w(F_o^2-F_c^2)^2] / \Sigma [w(F_o^2)^2] \}^{1/2}$; $R1 = \Sigma | |F_o| - |F_c| | / \Sigma |F_o|$ *GooF = $S = \{\Sigma [w(F_o^2 - F_c^2)^2] / (n-p)$

dinucleotide phosphate (NADPH) to reduce the tetrazolium, MTT salt into insoluble formazan crystals. Cell viability was measured by the similar assay conditions in DL and in peripheral blood mononuclear cells (PBMC) [(normal cells)] as discussed in the Chapter 2 according to the instructions in the Cell Proliferation Kit.[33] We have used different doses (0, 0.01, 0.1, 0.5, 1, 5 and 10 μM) of the complexes with 10 μL of the MTT labeling reagent (5 mg/mL in phosphate-buffered saline) and added into each well except the empty wells. The microtiter plate was then incubated for four hours under 5% CO_2 and 95% air at 37ºC. Following that, 100 μL of the DMSO was poured into each well with gentle shaking. The plate was checked for complete solubilization of the crystals. The mean absorbance for the soluble product of MTT reaction was expressed as a percentage of the control untreated well absorbance and plotted versus drug concentration.

4.2.8 Cell proliferation and apoptosis assay

Apoptosis inducing potential of the complexes (**7**, **8** and **9**) was assessed by using acridine orange/ethidium bromide (AO/EB) double staining method.[34] Control and treated cancer cells were collected after 24 hours of treatment, washed with PBS (phosphate-buffered saline) and to the cell suspension; 20 μL of AO/EB dye mixture (100 μg/mL of each dye in distilled water) was added, mixed gently and incubated for 5 min in dark. The cells were thoroughly examined under fluorescence microscope and photographed. About 1000 cells were analyzed and the percentage of apoptotic nuclei was determined for three independent experiments based on differential colouring pattern of nuclei. Viable cells were identified by bright uniform green nuclei with organized structures; apoptotic cells contain condensed or fragmented chromatin with red or orange nuclei.[35]

4.2.9 Molecular docking

The possible molecular interactions between the complexes **7**, **8** and **9** and anti-apoptotic target protein, BCL-2 were studied using Molegro Virtual Docker (MVD 2010.4.0) software for Windows[36] as discussed in Chapter 2. The molecular arrangement and geometry of the compounds **7**, **8** and **9** were fully optimized using the semi-empirical quantum chemistry method (Parametric Method 3). The docking

parameters were run using a GRID of 15 Å in radius and 0.30 in resolution with number of runs: 10 runs; algorithm: Moldock SE; maximum interactions: 1500; maximum population size: 50; maximum steps: 300; neighbour distance factor: 1.00; maximum number of poses returned: 5 to cover the ligand-biding site of the proteins structure.[37] Protein-ligand binding site was further analyzed and visualized by using BIOVIA Discovery Studio (http://3dsbiovia.com/products/) and Chimera (https://www.cgl.ucsf.edu/chimera/) software.[38]

4.2.10 Pharmacophore modelling

Pharmacophore models of the complexes **7**, **8** and **9** were generated using Ligandscout software which demonstrated Structure Activity Relationship (SAR).[39] After performing molecular docking simulation, the best docking orientations (pose) were loaded into Ligandscout software and key pharmacophore features were identified including H-bond donor, H-bond acceptor, hydrophobic, aromatic, halogen bond donor, positively and negatively ionizable groups.[39]

4.2.11 Statistical analysis

Data are expressed as mean ± standard deviation (S.D.). To determine the significance of the differences among the groups, one-way ANOVA was performed followed by Post hoc test. $P \leq 0.05$ was considered to be statistically significant.

4.3 RESULTS AND DISCUSSION

4.3.1 Synthesis and general aspects

The complexes $[Co(3\text{-}CNpy)_2(2\text{-}ClBz)_2(H_2O)_2]$ (**7**), $[Mn(3\text{-}CNpy)_2(2\text{-}ClBz)_2(H_2O)_2]$ (**8**) and $[Zn(3\text{-}CNpy)_2(2\text{-}ClBz)_2(H_2O)_2]$ (**9**) have been isolated in high yield by reacting one equivalent of the respective metal chlorides, $MCl_2 \cdot nH_2O$ with two equivalents of *3-CNpy* and two equivalents of sodium 2-chlorobenzoate in water. Complexes **7**, **8** and **9** are moderately soluble in water; however their solubility in common organic solvents is low. The complexes **7** and **8** show room temperature μ_{eff} values of 3.86 BM and 5.81 BM respectively and confirm the presence of unpaired electrons in the high spin states of the metal centers.[40]

4.3.2 Spectral properties

4.3.2.1 FT-IR Spectroscopy

FT-IR spectra of the complexes **7**, **8** and **9** (KBr pellets) were recorded in the region 4000-500 cm^{-1} (**Figure 4.1**). Being isostructural, the complexes **7**, **8** and **9** are found to have similar and very close peaks. The strong and broad bands at 3449, 3456 and 3476 cm^{-1} are assigned to the symmetric and anti-symmetric ν(OH) stretching vibrations of coordinated water molecules of **7**, **8** and **9** respectively.[41] The absence of bands at around 1730 cm^{-1} for them indicates that the carboxyl groups get completely de-protonated to the respective anions upon coordination to the metal ions.[42] The differences between the asymmetric stretching, $\nu_{as}(COO^{-})$ and symmetric stretching vibration bands, $\nu_{s}(COO^{-})$ for all the three complexes are observed above 200 cm^{-1} which indicates monodentate binding of the carboxyl group of *2-ClBz* to the respective metal centres.[43] B. Farkas *et al*. have also confirmed the monodentate coordination of the carbolxylate moiety to the metal centers for similar complexes.[44]

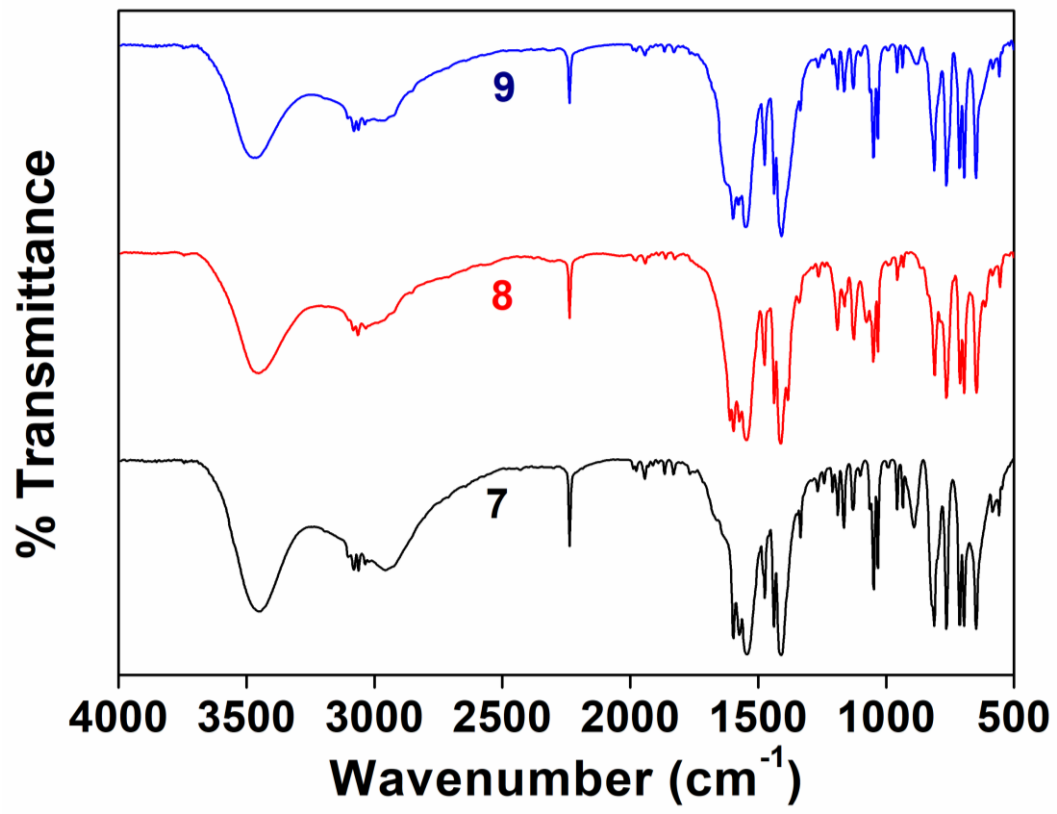

Figure 4.1 FT-IR spectra of complexes **7**, **8** and **9**.

The moderately strong vibrations at around 2236 cm^{-1} in all the complexes can be assigned to the nitrile stretching frequency, ν(C≡N) of *3-CNpy* moiety. M. Heine *et al*. have also reported similar absorption for the nitrile stretching frequency, ν(C≡N) of *3-CNpy* moiety in the coordination polymers of formula $[M(II)Cl_2(3\text{-}CNpy)_2]_n$ (M = Mn, Fe, Co, Ni, Cu, Zn).[45] The position of this band in the complexes **7**, **8** and **9** remains almost unaffected from that of the free base, implying non-coordination of the nitrile group of the *3-CNpy*.[46] These observations are well consistent with their structures as determined by single crystal XRD analyses.

4.3.2.2 Electronic Spectroscopy

The electronic spectra of all the three complexes **7**, **8** and **9** are represented in **Figures 4.2-4.4**. We can expect three ligand field bands for the high-spin octahedral Co(II) complex *viz*. $^4T_{1g}(F)\rightarrow{}^4T_{2g}(F)$ (ν_1), $^4T_{1g}(F)\rightarrow{}^4A_{2g}(F)$ (ν_2) and $^4T_{1g}(F)\rightarrow{}^4T_{1g}(P)$ (ν_3). In the UV-Vis-NIR spectrum [**Figure 4.2(a)**] of compound **7**, the first band occurs at 1131 nm, the third band is seen at 464 nm, and the ν_2 band due to $^4T_{1g}(F)\rightarrow{}^4A_{2g}(F)$ appears at 509 nm because of a two-electron transition.[47]

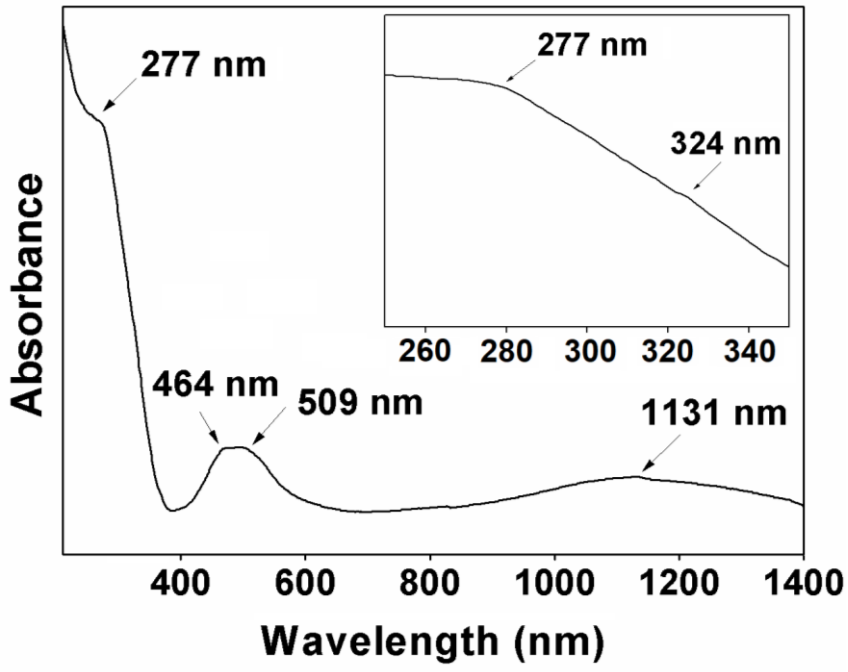

(**a**)

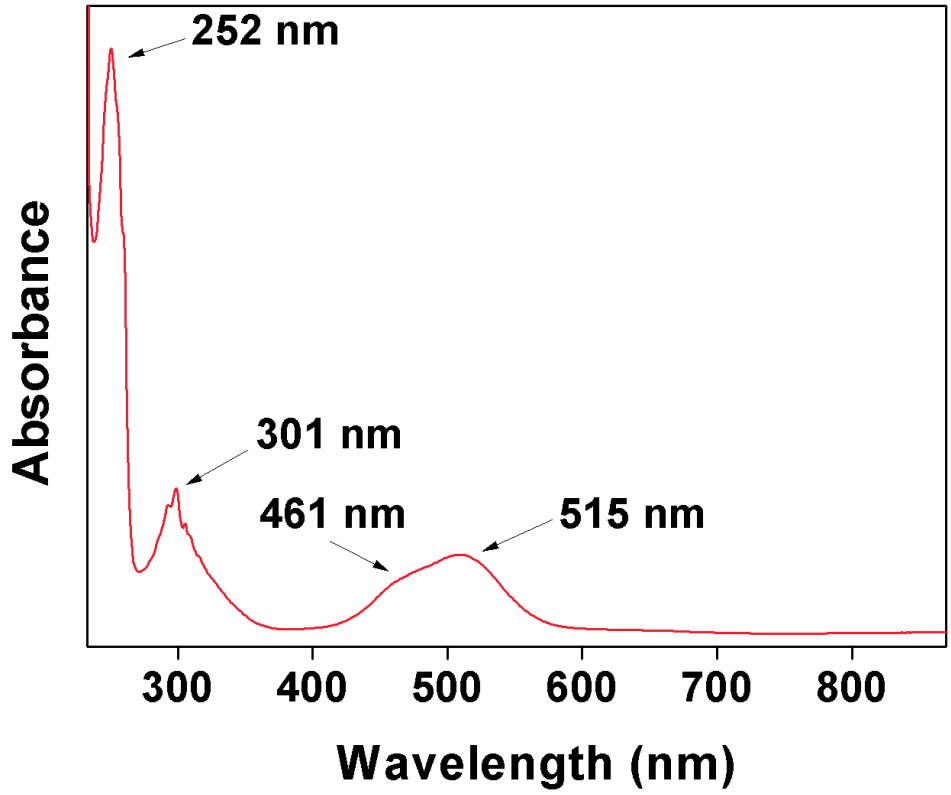

(**b**)

Figure 4.2(**a**) UV-Vis-NIR spectrum of $[Co(3\text{-}CNpy)_2(2\text{-}ClBz)_2(H_2O)_2]$ (**7**); (**b**) UV-Vis spectrum of $[Co(3\text{-}CNpy)_2(2\text{-}ClBz)_2(H_2O)_2]$ (**7**) in water.

However, the spectrum in water [**Figure 4.2**(**b**)] shows weak absorption bands at 461 and 515 nm, assigned to $^4T_{1g}(F) \rightarrow {}^4T_{1g}(P)$ (ν_3) and $^4T_{1g}(F) \rightarrow {}^4A_{2g}(F)$ (ν_2) transitions respectively. The NIR band is not seen in the solution spectrum because of the limit in the wavelength window of the spectrophotometer used.[48] K. Singh *et al*. have also reported similar ligand field bands for the high-spin octahedral Co(II) complex having molecular formula $Co(L)_2 \cdot 2H_2O$ [where, HL = 4-(5-Nitrofurfuralideamino)-5-mercapto-3-methyl-1,2,4-triazole].[49]

The electronic spectra of the complexes **8** and **9** are shown in **Figure 4.3** and **Figure 4.4** respectively. The spectra of compound **8** in the solid and aqueous phases show no d-d band (**Figure 4.3**), because for Mn^{2+}, which is a d^5 system, all electronic transitions from the $^6A_{1g}$ ground state are doubly forbidden.[50] The absorption at 214 nm in the aqueous phase can be assigned to the $\pi \rightarrow \pi^*$ absorption of aromatic ligands,

whereas the shoulder around 265 nm is attributed to the LMCT [O (or N)→Mn)] transition.[51] In the UV-Vis-NIR spectrum (**Figure 4.3**) however, these absorption peaks are observed at 215 and 268 nm respectively.

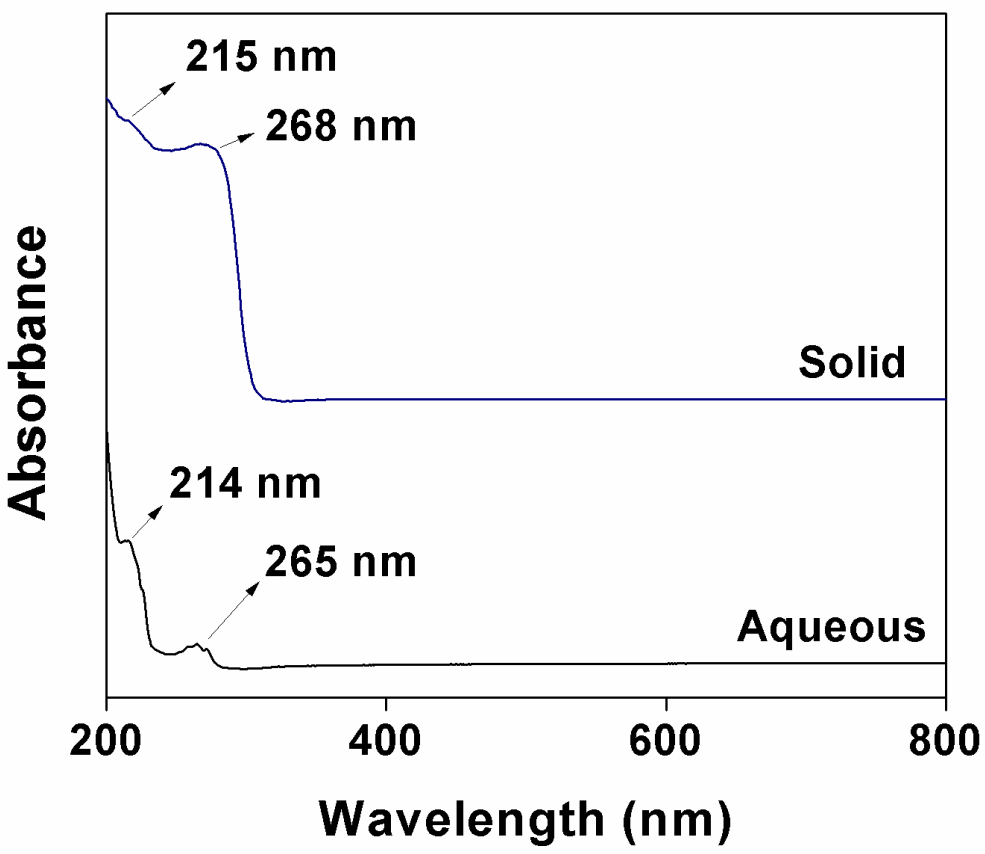

Figure 4.3 Electronic spectra of $[Mn(3\text{-}CNpy)_2(2\text{-}ClBz)_2(H_2O)_2]$ (**8**).

In the wavelength range 212-268 nm, characteristic absorptions in the solid and aqueous phases for compound **9** are observed due to π–π* and n–π* transitions of the pyridine rings of *3-CNpy* and the *2-ClBz* moieties (**Figure 4.4**).[52] No spectral band in the visible region for compound **9** in both the phases can be attributed to the d^{10} configuration of the Zn(II) centre, which does not allow any electronic transition to the higher excited electronic states.[53] Kumar *et al*. have also reported similar electronic spectra for Mn(II) and Zn(II) complexes with Schiff base, 4-(2,4-diamino-benzaldimino)-3,5-dimercapto-1,2,4-triazole.[54] The electronic spectral analyses for the complexes **7**, **8** and **9** in the solid and in the aqueous solution do not show marked differences and therefore, it may be assumed that the bonding modes of ligands to the

metal centers as well as the geometries of the complexes remain same in both the phases.[55]

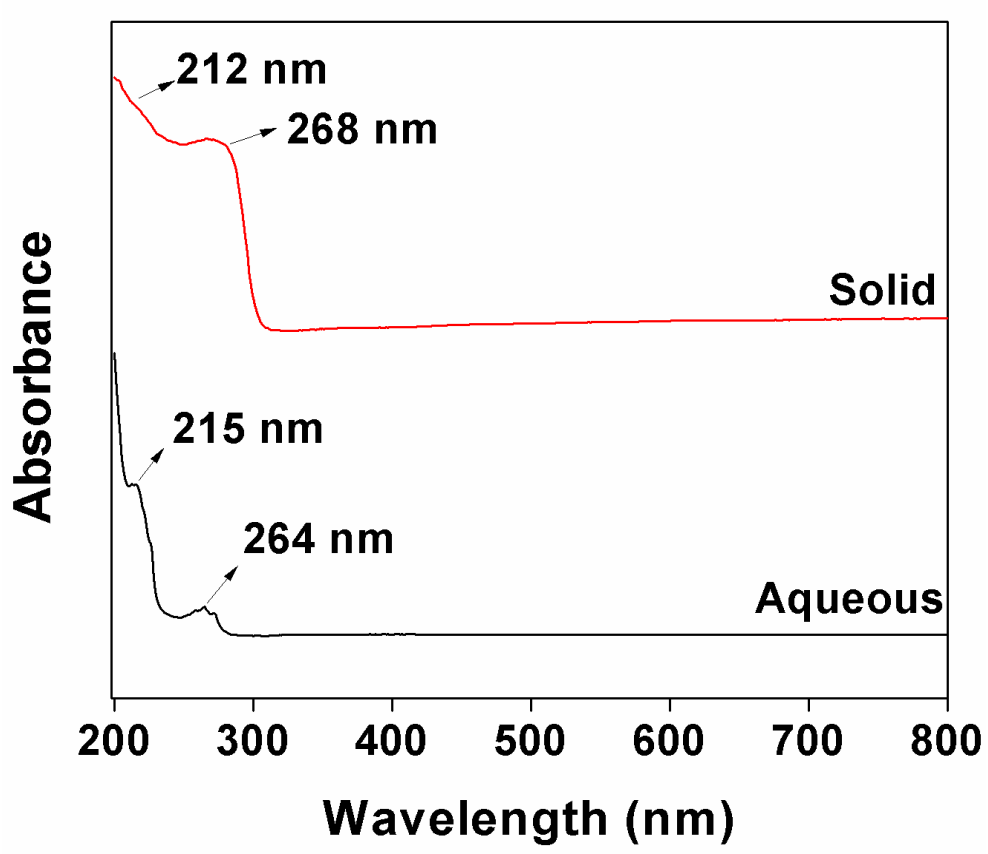

Figure 4.4 Electronic spectra of $[Zn(3\text{-}CNpy)_2(2\text{-}ClBz)_2(H_2O)_2]$ (**9**).

4.3.3 Crystal structures

Single-crystal X-ray diffraction analysis reveals that **7**, **8** and **9** are isostructural complexes and crystallize in the same monoclinic space group $P2_1/c$ with similar unit cell parameters (**Table 4.1**). Their selected bond lengths (Å) and bond angles (°) are presented in **Table 4.2**. As shown in **Figures 4.5**, **4.6** and **4.7**, complexes **7**, **8** and **9** are composed of mononuclear M(II) metal [M = Co(**7**), Mn(**8**) and Zn(**9**)] centers and their charge- compensated by two *2-ClBz* anions coordinated to the metal along with two *3-CNpy* moieties that results in distorted octahedral geometries. The metal ions of the coordination complexes lie on a two-fold axis of symmetry; therefore half of their molecules constitute the respective asymmetric units. The equatorial plane of **7**, **8** and **9** are defined by O2 and O2# from two of the coordinated *2-ClBz* ligands and N1 and N1#

from *3-CNpy* ligands. O1 and O1# from coordinated water molecules are positioned at the axial sites with bond angles of about 180° for the complexes **7**, **8** and **9**. The sum of the bond angles of O2–Co1–N1 [88.74(1)°], O2–Co1–N1# [91.25(1)°], O2#–Co1–N1# [88.74(1)°] and N1–Co1–O2# (91.25(1)°]; O2–Mn1–N1 [88.89(1)°], O2–Mn1–N1# [91.11(1)°], O2#–Mn1–N1# [88.89(1)°] and N1–Mn1–O2# (91.11(1)°]; O2–Zn1–N1 [88.12(1)°], O2–Zn1–N1# [90.86(1)°], O2#–Zn1–N1# [90.86(1)°] and N1–Zn1–O2# [89.14(1)°] are 359.98°, 360° and 359.98° respectively shows that O2, N1, O2#, and N1# atoms are almost coplanar (mean r.m.s. deviation of 0.0281 Å, 0.0280 Å and 0.0282 respectively for compounds **7**, **8** and **9**). A comparative study shows that the average Co1–O, Co1–N, Mn1–O, Mn1–N and Zn1–O, Zn1–N bond distances (**Table 4.2**) are almost consistent with the previously reported Co(II), Mn(II) and Zn(II) complexes.[56]

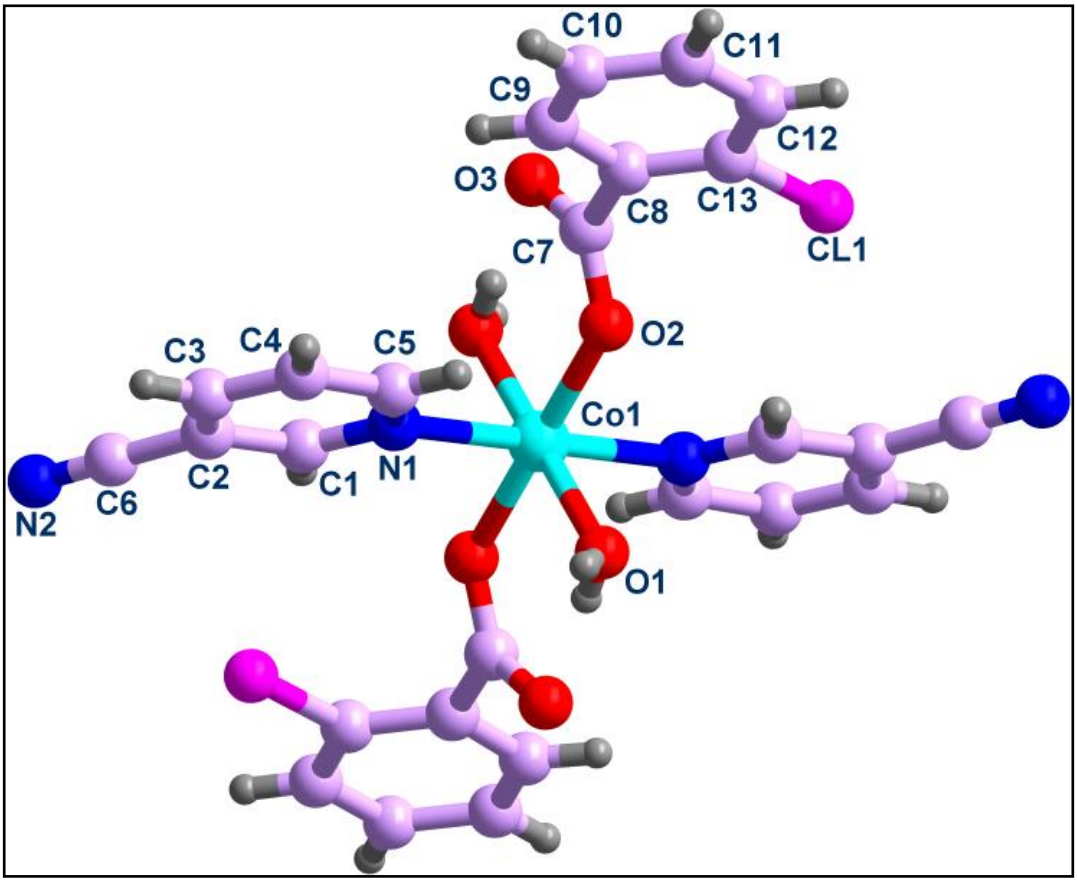

Figure 4.5 Molecular structure of $[Co(3\text{-}CNpy)_2(2\text{-}ClBz)_2(H_2O)_2]$ (**7**).

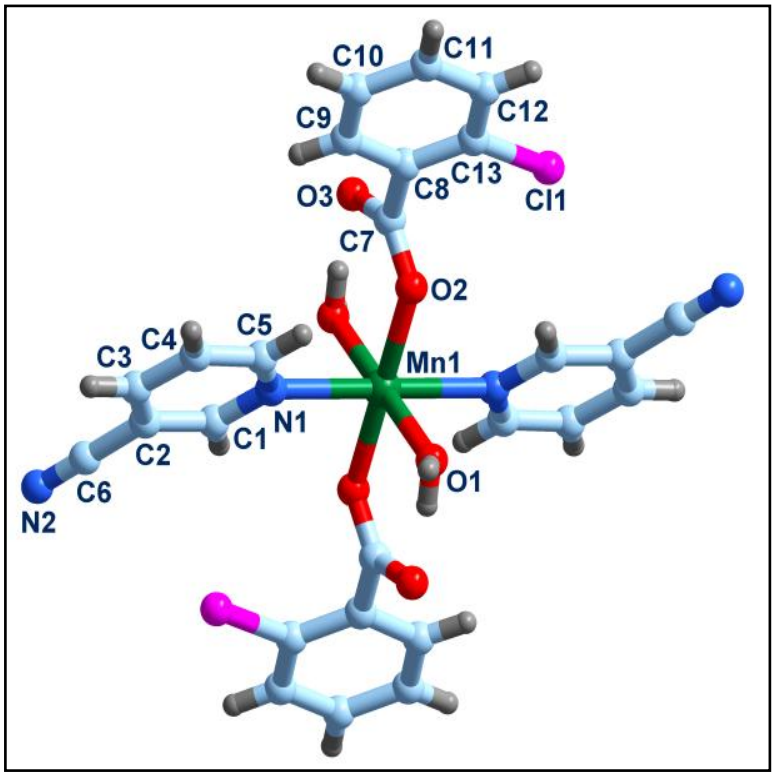

Figure 4.6 Molecular structure of $[Mn(3\text{-}CNpy)_2(2\text{-}ClBz)_2(H_2O)_2]$ (**8**).

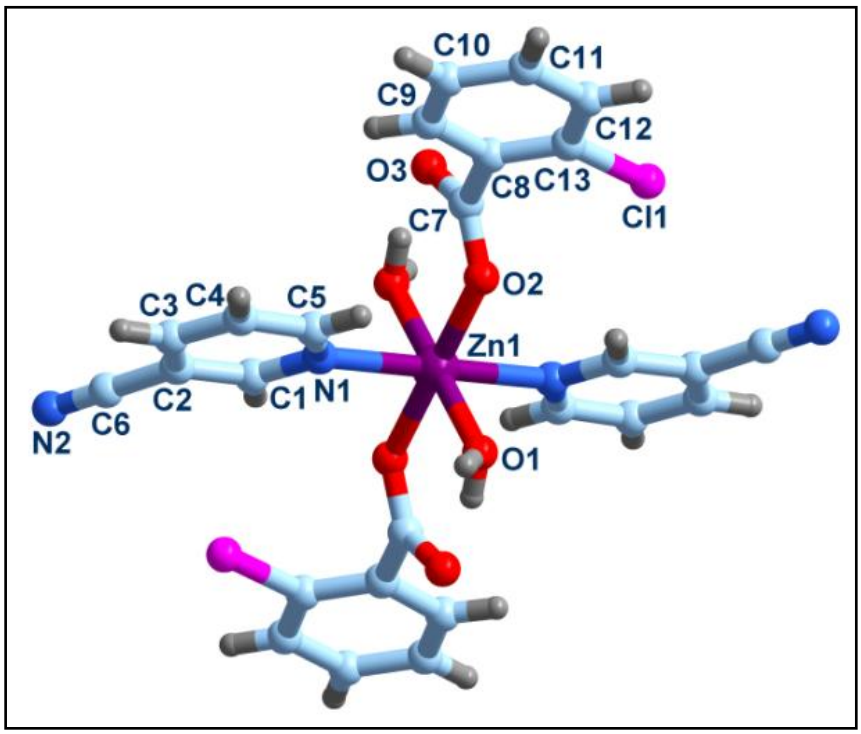

Figure 4.7 Molecular structure of $[Zn(3\text{-}CNpy)_2(2\text{-}ClBz)_2(H_2O)_2]$ (**9**).

Table 4.2 Selected bond lengths (Å) and bond angles (°) for **7**, **8** and **9**.

Bond length	**7**	**8**	**9**
M–O1	2.102(1)	2.173(1)	2.113(1)
M–O2	2.078	2.147(5)	2.084(5)
M–N1	2.185	2.305(6)	2.189(6)
Bond angle	**7**	**8**	**9**
O1–M–O2	88.230(1)	90.46(1)	92.23(1)
O1–M–N1	93.359(1)	92.22(1)	86.86(1)
O1–M–O2^{i}	91.770(1)	89.53(1)	87.76(1)
O1–M–N1^{i}	86.641(1)	87.78(1)	93.138(1)
O2–M–N1	88.745(1)	91.11(1)	89.14(1)
O2–M–N1^{i}	91.255(1)	88.89(1)	90.86(1)

Symmetry codes: (i) 1–x, –y, 1–z for **7**; (i) – x, –y, 1–z for **8**; (i) 2–x, –y, 2–z for **9**

In the crystal structure of the complexes **7**, **8** and **9**, hydrogen bondings as well as π–π stacking interactions are observed among the monomeric units. The hydrogen bond details are presented in **Table 4.3**. Since the complexes **7**, **8** and **9** are isostructural (**Figures 4.5-4.7**), the discussions here of crystal structures and figures will be in terms of complex **7**.

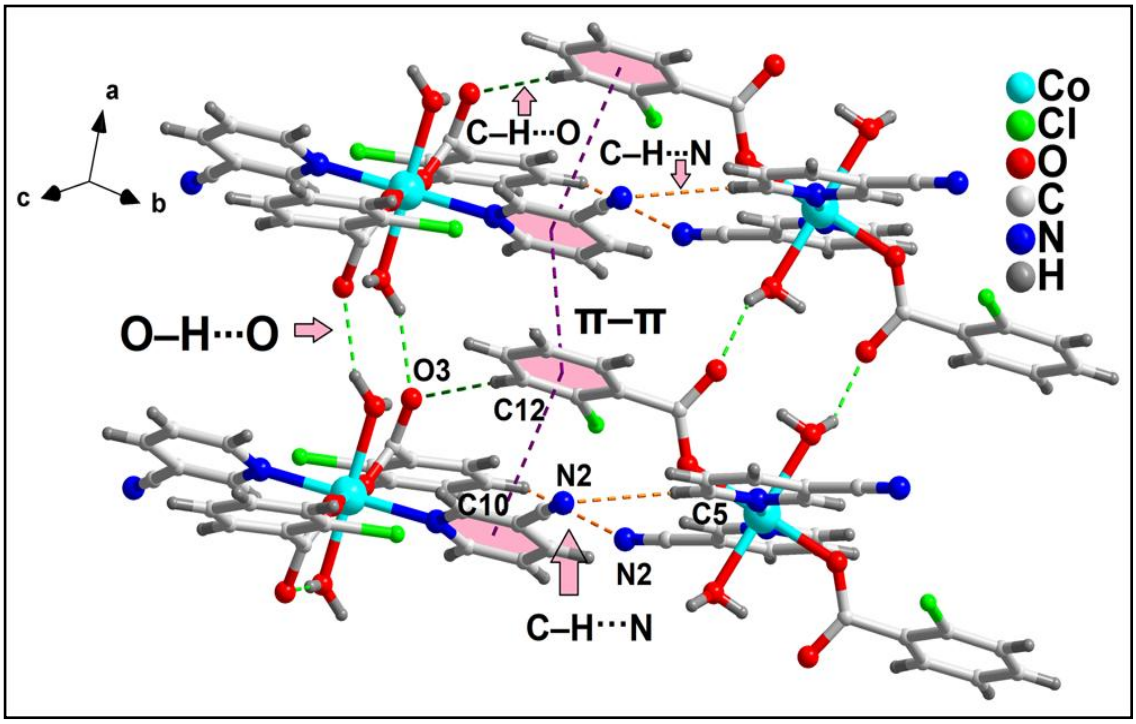

Figure 4.8 Supramolecular interactions between the monomeric units of [Co(3-CNpy)$_2$(2-ClBz)$_2$(H$_2$O)$_2$] (**7**) via C–H···N, C–H···O, O–H···O and π–π stacking interactions along the crystallographic *ac* plane.

Along the *ac* plane, the neighbouring molecules of **7** are interconnected by C–H···N, C–H···O, O–H···O and π–π stacking interactions (**Figure 4.8**). The N2 atom of neighbouring *3-CNpy* moiety of the monomeric unit is involved in C–H···N interaction with –CH moiety of adjacent monomeric unit having C10–H10···N2 and C5–H5···N2 distances of 2.793(1) and 2.860(1) Å respectively. On the other hand, O3 atom of *2-ClBz* moiety is also involved in C–H···O interaction with –CH moiety of *2-ClBz* of another monomeric unit having C12–H12···O3 distance of 2.480(1) Å. Phenyl ring of one monomeric unit is involved in π–π stacking interaction with the pyridine ring of another monomeric unit with the centroid-centroid separation of 4.001(1) Å.[57] E. Tocana *et al.* have also reported similar π–π contacts involving pyridine and phenyl rings in the complex $[Ni(phen)_2(H_2O)_2](ClO_4)_2$ [where, phen = 1,10-phenanthroline] having centroid-centroid separation of 4.002 Å.[58]

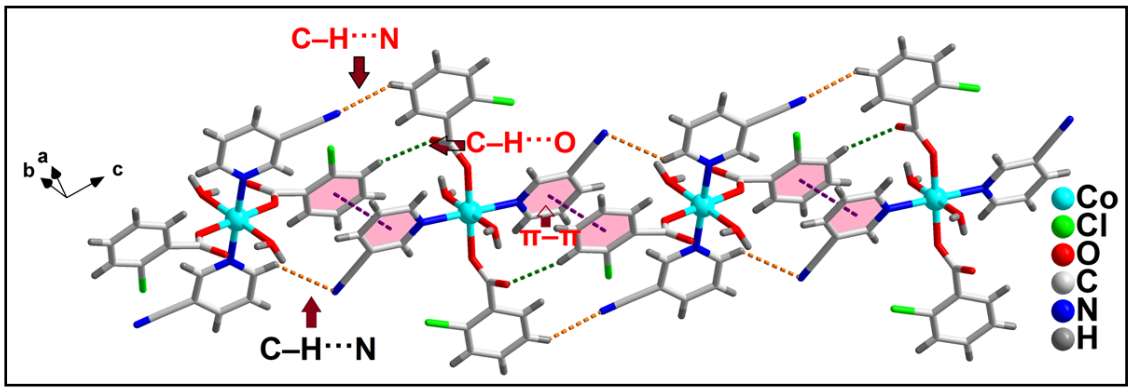

Figure 4.9 Weak hydrogen-bonded 1D chain of complex **7** stabilized by π–π staking interactions.

Along the *ab* plane, the neighbouring molecules of **7** are interconnected by C–H···O hydrogen bonds with donor–acceptor distance of 2.480 Å, involving the coordinated *2-ClBz* to form 1D hydrogen-bonded chains in the crystal structure (**Figure 4.9**). Additional reinforcement within this chain is provided by C–H···N and π–π interactions. The free nitrile moieties from *3-CNpy* are involved in two types of C–H···N hydrogen bonds, where they accept hydrogen bonds from C5H5 and C10H10 moieties from neighbouring *3-CNpy* and *2-ClBz* groups respectively with donor–acceptor distances of 3.507 and 3.613 Å. This type of C–H···N hydrogen bonds involving N atom of nitrile group and H atom of aromatic ring in the coordination complexes of formula

[{Cu(dicnq)Br}2H_2btca]1.7(CH_3OH) [where, H_2btca = 1,2,4,5-benzenetetracarboxylate, dicnq = 6,7-dicyanodipyridoquinoxaline] and [Cd_2(4-NO_2Bz)$_4$(2-CNpy)$_4$] [where, 4-NO_2Bz = 4-nitrobenzoate, 2-CNpy = 2-cyanopyridine] were reported by Maria D. Stephenson and Michaele J. Hardie[59] and T. Hokelek *et al.*[60] respectively with similar donor–acceptor distances. These interactions place the molecules within the supramolecular chain in such a way that the phenyl ring of *2-ClBz* group of one mononuclear complex unit points toward the pyridyl π-cloud of *3-CNpy* ligand of the adjacent complex unit, thereby giving rise to π-π stacking interactions with centroid-centroid separation of 4.001 Å.

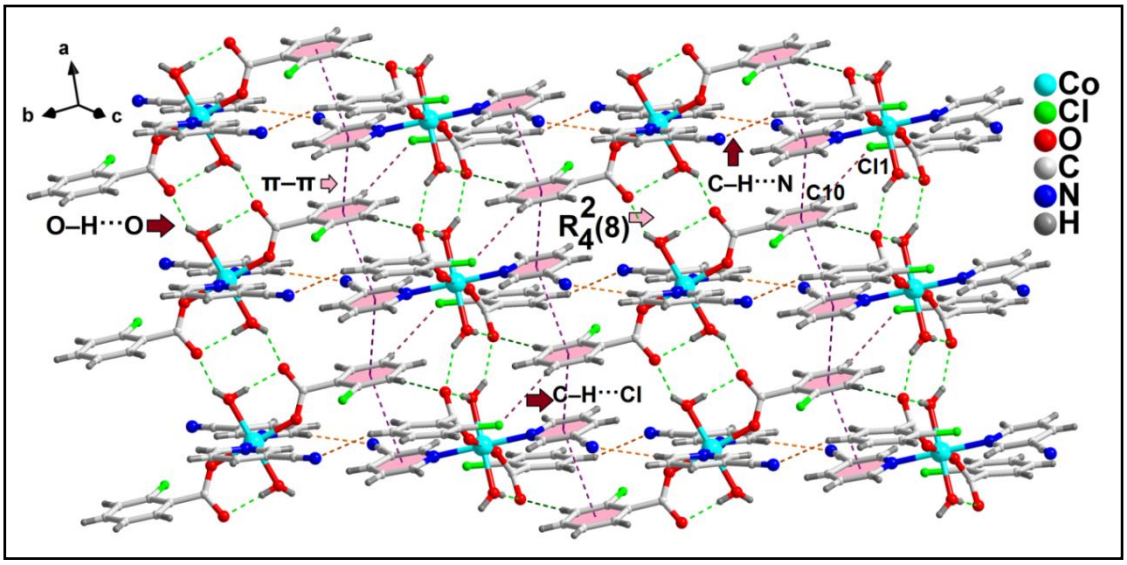

Figure 4.10 Formation of layered assembly of [Co(3-CNpy)$_2$(2-ClBz)$_2$(H_2O)$_2$] (**7**) along the *ac* plane, generated through $R_4^2(8)$ hydrogen bonding synthons.

Two adjacent 1D chains in the crystal structure of complex **7** are connected by O–H···O hydrogen bonds, assisted by coordinated aqua ligand and uncoordinated carboxylic O atom of *2-ClBz* group. An eight membered supramolecular ring motif, expressed as $R_4^2(8)$ in the graph-set notation of Etter[61], is formed by the cooperative interaction between the pairs of H_2O molecules and uncoordinated carboxylic O atoms, centro-symmetrically connected by O1–H1A···O3 and O1–H1B···O3 interactions with H···O distances of 1.860 and 2.014 Å respectively (**Figure 4.10**). These supramolecular rings in **7** are repeated along the *a*-direction to complete the 2D supramolecular framework in the *ac* plane. The layered architecture of **7** is further reinforced by

C–H···Cl and π–π stacking interactions. The C–H···Cl interaction involves the C10H10 moiety of *2-ClBz* group of one chain and the Cl1 atom of the same group from an adjacent chain. The bond distance between H10 and Cl1 is 3.030 Å, the bond angle of C10–H10–Cl1 is 120.94°, which is close to the preferred minimum hydrogen bond angle of 121°. The distance between C10 and Cl1 is 3.598 Å, which is similar to the sum of the van der Waals radii of C and Cl. A. C. Moro *et al.* have reported such C–H···Cl interactions with similar bond parameters in the complex $[PdCl_2(PPh_3)(tu)]$ (where, PPh_3 = triphenylphosphine, tu = thiourea).[62] Moreover, aromatic π–π stacking interactions are also observed between two neighbouring chains involving the adjacent pyridine rings of *3-CNpy* and phenyl rings of *2-ClBz* having the centroid-centroid separations of 4.061 and 3.801 Å respectively. These layers stack together along the crystallographic *c*-direction via a number of supramolecular contacts to generate a 3D architecture involving 1D channels along the crystallographic *c*-direction (**Figure 4.11**).

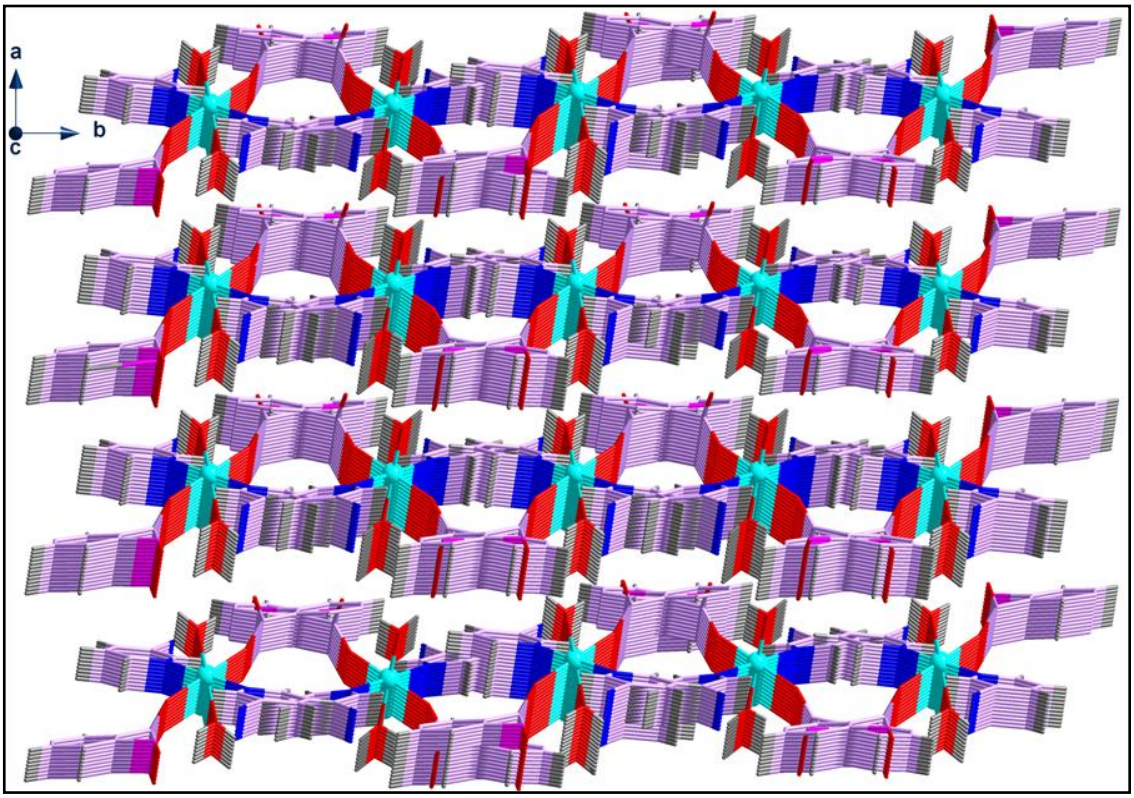

Figure 4.11 View of 3D supramolecular architecture of $[Co(3\text{-}CNpy)_2(2\text{-}ClBz)_2(H_2O)_2]$ (**7**) involving 1D channels along the crystallographic *c*-direction.

The isostructural complexes **8** and **9** also show similar networks as complex **7**. However, subtle structural differences between the complexes **7**, **8** and **9** in bond lengths, bond angles, hydrogen bonds and torsion angles may be due to the different atomic radii of Co(II), Mn(II) and Zn(II) ions respectively.

Table 4.3 Selected hydrogen bond distances (Å) and angles (°) for **7**, **8** and **9**.

D–H···A		d(D–H)	d(D–A)	d(H···A)	<(DHA)	Symmetry
O1–H1A···O3	**7**	0.798	2.658	1.860 (0)	178.24 (3)	–x+1,–y,–z+1
	8	0.830	2.731	1.951 (2)	156.27 (10)	–x,–y,–z+1
	9	0.906	2.761	1.932 (17)	151.27 (89)	–x+1,–y,–z+2
O1–H1B···O3	**7**	0.843	2.770	2.014 (1)	148.89 (2)	x–1,+y,+z
	8	0.864	2.668	1.828 (15)	163.58 (11)	x,y,z
	9	0.829	2.649	1.865 (14)	157.15 (98)	–x+1,–y,–z+2
C5–H5···N2	**7**	0.930	3.507	2.860 (1)	127.70 (2)	x,y+1/2,+z+12
	8	0.929	3.511	2.860 (29)	128.58 (13)	x,–y–1/2,+z–1/2
	9	0.930	3.506	2.858 (27)	127.75 (11)	x,–y–1/2,+z–1/2
C10–H10···N2	**7**	0.930	3.613	2.796 (1)	145.15 (2)	–x+1,+y+1/2,–z+1/2
	8	0.930	3.589	2.767 (24)	147.92 (13)	x,–y+1/2,+z–1/2
	9	0.930	3.593	2.776 (22)	147.14 (13)	–x+2,+y–1/2, z+1/2+2
C11–H11···O1	**7**	0.930	3.438	2.826 (1)	124.42 (4)	–x+1,+y+1/2,–z+1/2+1
	8	0.931	3.452	2.853 (18)	123.24 (13)	x,–y+1/2,+z+1/2
	9	0.930	3.419	2.818 (16)	123.39 (12)	x,–y–1/2,+z–1/2
C12–H12···O3	**7**	0.930	3.394	2.481 (1)	167.14 (5)	x,–y+1/2,+z+1/2
	8	0.929	3.510	2.596 (21)	167.66 (12)	x,–y+1/2,+z+1/2
	9	0.930	3.438	2.525 (18)	167.65 (11)	x,–y–1/2,+z–1/2

4.3.4 Isostructurality of compounds 7, 8 and 9

The crystal structure analysis of the compounds **7**, **8** and **9** indicates that the compounds are quite analogous with one another, because these three compounds differ only on the basis of the central metal ions present in them. Such structurally analogous compounds belong to the same structure type and can be termed as isostructural.

The isostructurality of the three compounds has been further evaluated according to the approach of Fábián and Kálmán as discussed in Chapter 2 in which two structures may be compared by a parameter called unit cell similarity index given by

$$\Pi = [(a+b+c)/(a'+b'+c')] - 1 \text{ where, } (a+b+c > a'+b'+c').$$

Here a, b, c and a', b', c' are the orthogonalized lattice parameters of the structures of the compounds being examined. If the structural similarity is very high, the Π value is expected to be practically equal to zero.[63] For compounds **7** and **8**, the value is found to be 0.00571, which corroborates the close structural similarity obtained from crystal structure analyses. The corresponding values for the structure pairs (**7**)/(**9**) and

(**8**)/(**9**) are found to be 0.00140 and 0.00712 respectively. The other two related parameters *viz.* mean elongation value ($\in$) and the so-called asphericity index (*A*) of the compounds have also been determined. The $\in$ value describes the difference in cell size,

$$\in = \left(V' - V\right)^{1/3} - 1,\ V' > V;$$

where, *V* and *V*′ are the volumes of the respective unit cells. For our structure pairs (**7**)/(**8**), (**7**)/(**9**) and (**8**)/(**9**), the difference in cell size ($\in$) values estimated are 0.00726, 0.00109 and 0.00836 respectively. On the other hand, asphericity index (*A*) accounts for the shape distortions, and is defined as,

$$A = (2/3)[1 - \sum\nolimits_{j>i}\{[(1+\in)M_i - 1] \times [(1+\in)M_j - 1]/3\in^2\}]^{1/2}$$

where, M_i's are the principal axes of matrix M, which gives the pure shear component of the transformation between the two crystallographic coordinate systems. The *A* values for the same structure pairs, *viz*. (**7**)/(**8**), (**7**)/(**9**) and (**8**)/(**9**) are found to be 0.52664, 3.20046 and 0.255268 respectively. In this regard, we can also express their product $\in A$ as the lattice distortion index and the observed values are 0.00382, 0.00349 and 0.00213 respectively.

The above quantities obtained for **7**, **8** and **9** clearly indicate the isostructurality of the three crystalline solids. B. K. Das *et al*. have also highlighted the isostructurality parameters of two isostructural coordination compounds of the formula $[M(II)(H_2O)_3(SO_4)(4\text{-}CNpy)_2]\cdot H_2O$ [where, M = Ni(II) and Co(II), 4-CNpy = 4-cyanopyridine].[64] The reported unit cell similarity index value for these two isostructural compounds is found to be 0.0046.

4.3.5 Powder X-ray Diffraction

In order to prove that the synthesized coordination solids *viz*. $[M(3\text{-}CNpy)_2(2\text{-}ClBz)_2(H_2O)_2]$ [M = Co(**7**), Mn(**8**) and Zn(**9**)] are true representatives of their bulk materials, their powder X-ray diffractions were recorded at room temperature. The experimental and the calculated powder X-ray diffraction patterns for compounds **7**, **8** and **9** (**Figures 4.12-4.14**) are in good agreement with each other which demonstrates that the compounds are true representatives of the bulk samples. The small line width of the Bragg reflections demonstrates the good crystallinity of the compounds.

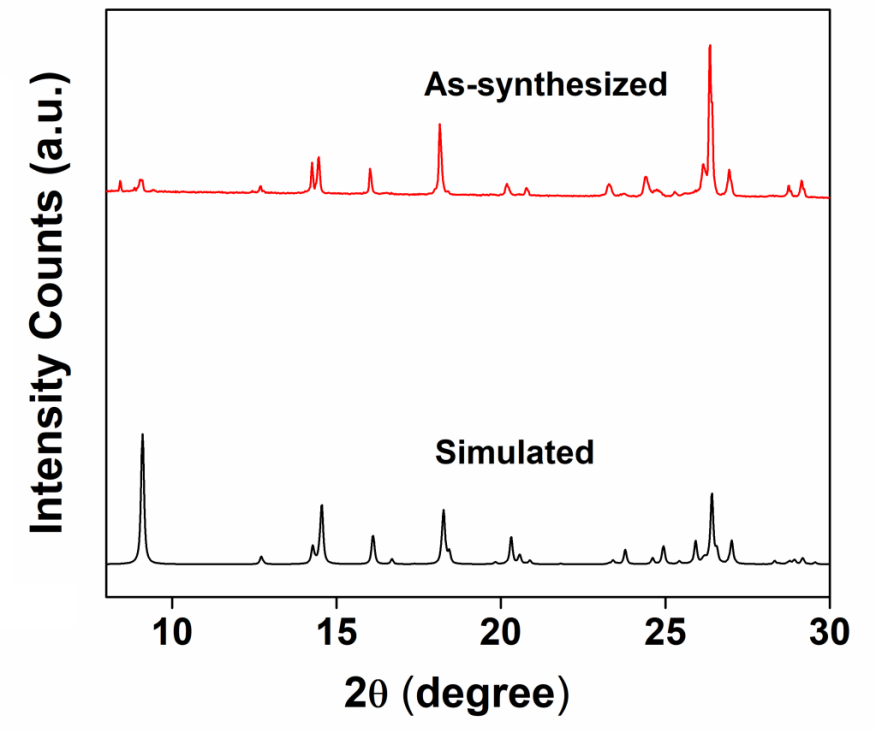

Figure 4.12 Powder X-ray diffraction patterns: as-synthesized (red) and simulated from MERCURY software (black) of $[Co(3\text{-}CNpy)_2(2\text{-}ClBz)_2(H_2O)_2]$ (**7**).

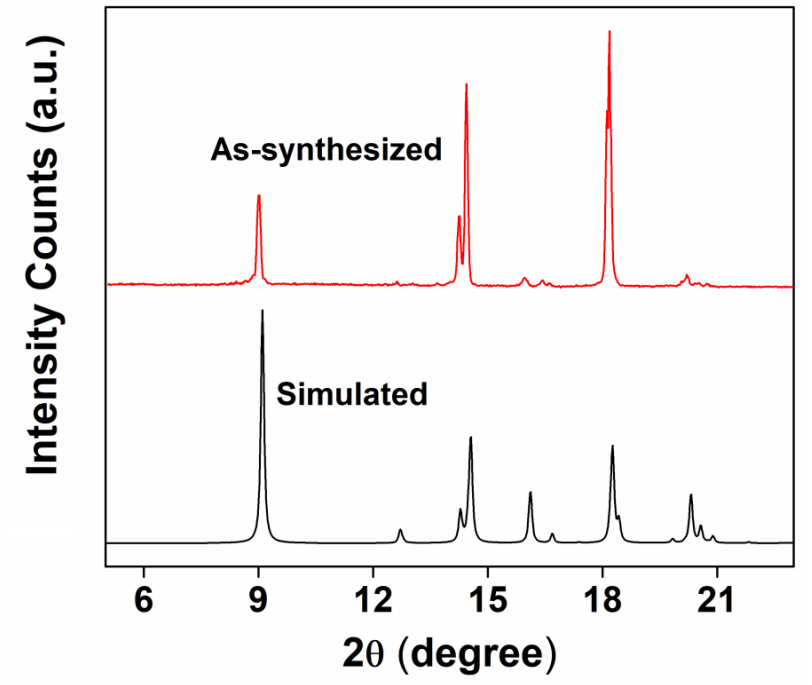

Figure 4.13 Powder X-ray diffraction patterns: as-synthesized (red) and simulated from MERCURY software (black) of $[Mn(3\text{-}CNpy)_2(2\text{-}ClBz)_2(H_2O)_2]$ (**8**).

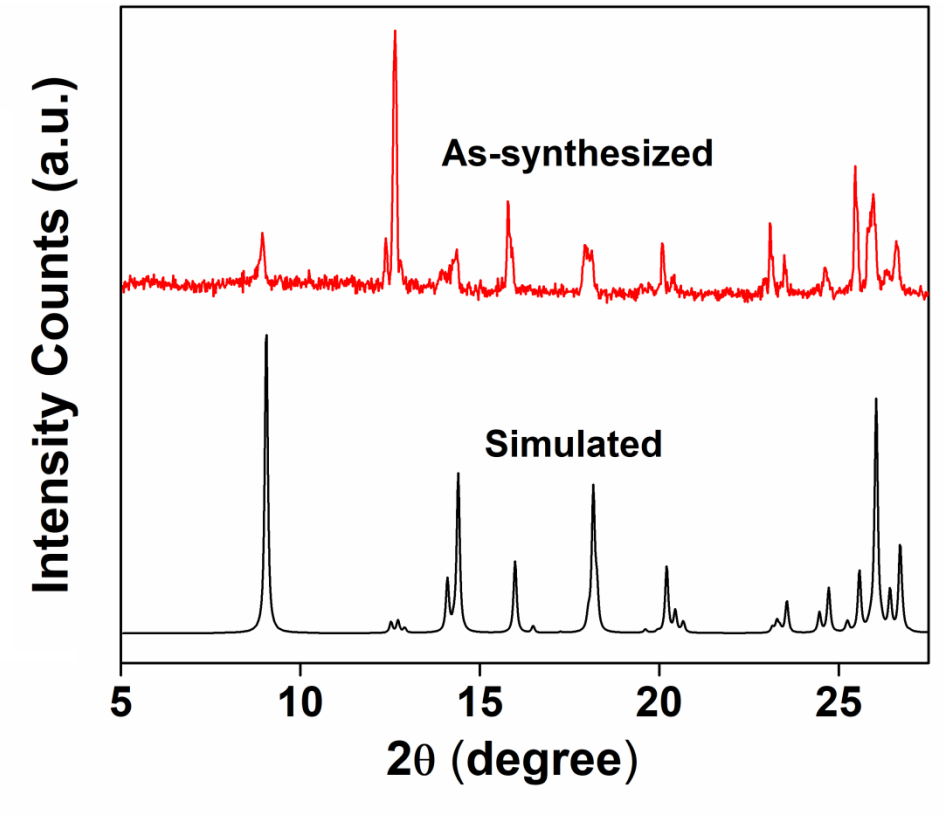

Figure 4.14 Powder X-ray diffraction patterns: as-synthesized (red) and simulated from MERCURY software (black) of $[Zn(3\text{-}CNpy)_2(2\text{-}ClBz)_2(H_2O)_2]$ (**9**).

Furthermore, the perfect fit of the as-synthesized and mercury simulated patterns indicates in favour of the closeness of the unit cell linear parameters.[65] Small differences in reflection intensities and peak positions are observed between the simulated and experimental patterns which can be attributed to the variation in crystal orientation or particle size of the powder sample.[66]

4.3.6 Theoretical Studies

The theoretical study is devoted to the analysis of the H-bonding and π–π stacking interactions that are crucial to understand the crystal packing of compounds **7**, **8** and **9** as described in **Figure 4.8**. Moreover, we are also interested in evaluating the effect of the metal center on the strength of the interactions. Initially, we have computed the MEP plotted onto the van der Waals surface (isosurface 0.001 a.u.) in order to investigate the electron poor and electron rich regions of complex **9** (**Figure 4.15**) as a

model of the three isostructural compounds. The most positive isocontour is located at one H-atom of the coordinated water molecule (+52 kcal/mol). This is due to the coordination of the water to the Zn(II) metal center that significantly increases the acidity of the H atoms. The most negative region is located at the uncoordinated O-atom of the anionic ligand, as expected. Therefore, a H-bond between both atoms is the most favoured electrostatically. This interaction is indeed observed in the solid state of the compounds (**Figure 4.8** and **Figure 4.16**). Moreover, further inspection of the MEP surface reveals that the value over the π-system of the *3-CNpy* ligand is positive (+20 kcal/mol) and negative over the π-system of *2-ClBz* ligand (-23 kcal/mol). Therefore, π-stacking interaction between both rings is also strongly favoured due to the donor-acceptor nature of the π-rings.

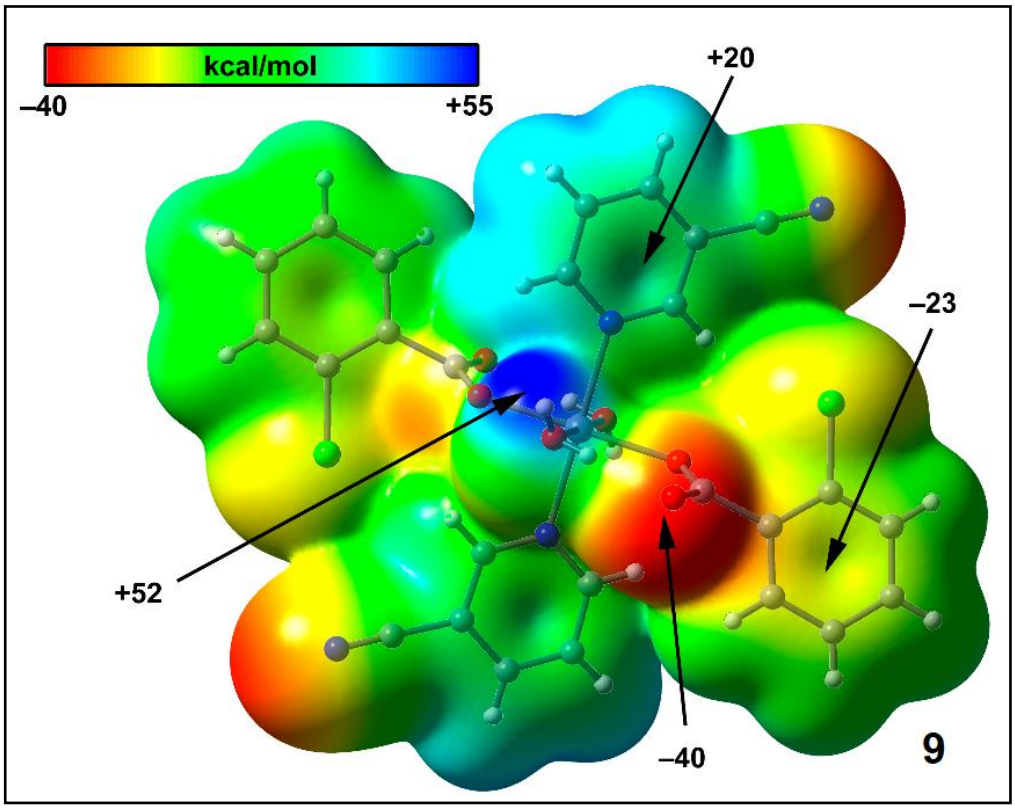

Figure 4.15 MEP surface of compound **9** at the B3LYP-D/def2-TZVP level of theory using the 0.001 a.u. isosurface. The values at selected points of the surface are indicated in kcal/mol.

We have analyzed the energetic features of the H-bonding and π-stacking interactions described for the compounds **7**, **8** and **9**. The interaction energies and

geometric features of the complexes are gathered in **Figure 4.16**. A partial view of the 2D sheet that is formed in the solid state (using complex **9** as model) in shown in **Figure 4.16(a)**, where two infinite 1D H-bonded chains are inter connected by means of π–π stacking contacts. The H-bonded assembly [**Figure 4.16(b)**, extracted from the infinite supramolecular chain] is more favourable than the π-stacked one [**Figure 4.16(c)**] with a binding energy that ranges from –17.7 to –15.9 kcal/mol. This large binding energy agrees well with the MEP analysis, since both the minimum and maximum values of MEP are located at the groups involved in these H-bonding interactions. Small geometric and energetic differences are observed among the three metals considered in this study, thus suggesting a similar ability to polarize the O–H group. The π–π dimer [**Figure 4.16(c)**] also presents moderately strong interaction energy (around –10 kcal/mol for all three compounds). This interaction energy is stronger than usual for complexes involving π-stacking between arenes due to the donor-acceptor nature of the rings in the complexes. Again, a negligible influence of the metal center on the interaction energy is observed.

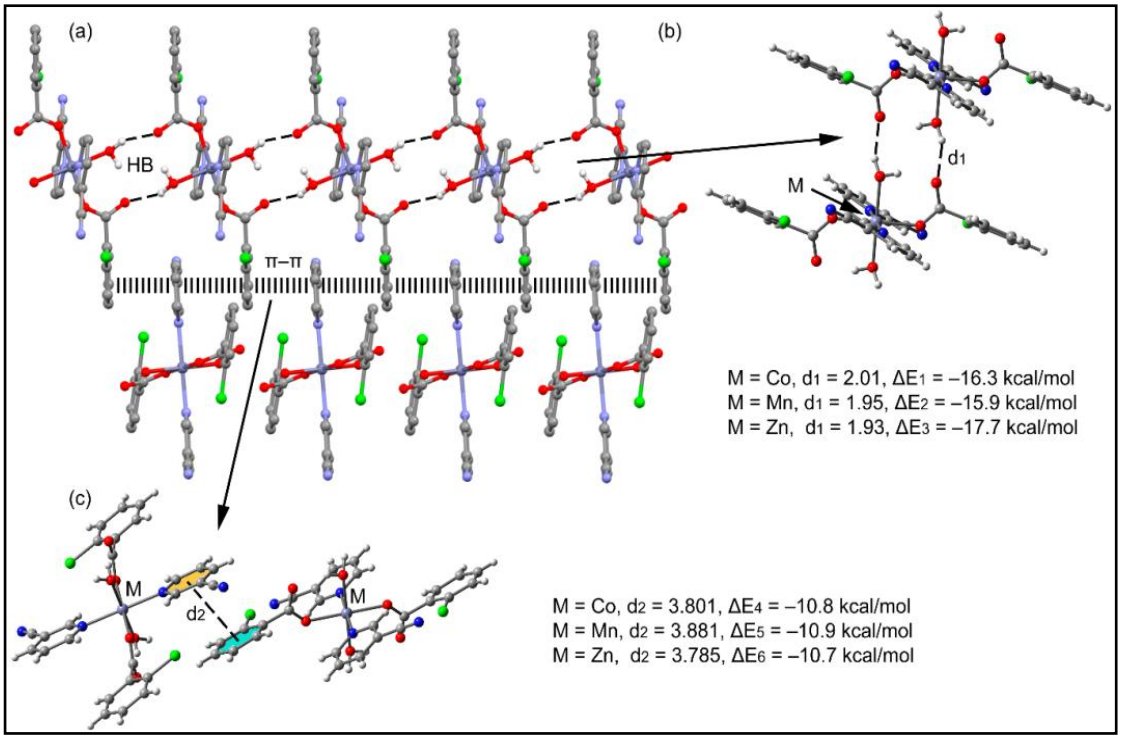

Figure 4.16 Partial view of the X-ray structure of complex **9** with indication of the H-bonded 1D supramolecular chain interconnected by means of π–π interactions.

In order to further characterize the H-bonding and π–π assemblies, we have used the NCI plot index. Non-covalent interactions are conveniently identified and visualized by the NCI index, because it allows an easy assessment of host-guest complementarity and the extent to which weak interactions stabilize a complex. We have computed the NCI plots for the H-bonding and π–π assemblies of compound **9** as a representative model, which are represented in **Figure 4.17**. Each H-bonding interaction is characterized by a small and blue isosurface located between the H-atom of the coordinated water molecule and the carboxylate O-atom [see **Figure 4.17**(**a**)], thus confirming the strong nature of these H-bonds in agreement with the MEP surface shown in **Figure 4.15**. For the π–π dimer [**Figure 4.17**(**b**)], a large green isosurface can be observed between both π-systems that embraces the whole aromatic rings, thus suggesting a large overlap of the aromatic rings. Moreover, two small and green isosurfaces are also present between two aromatic C–H bonds and the O atoms of the carboxylate that reveal the existence of ancillary C–H···O bonding interactions also contribute to the stabilization of the assembly.

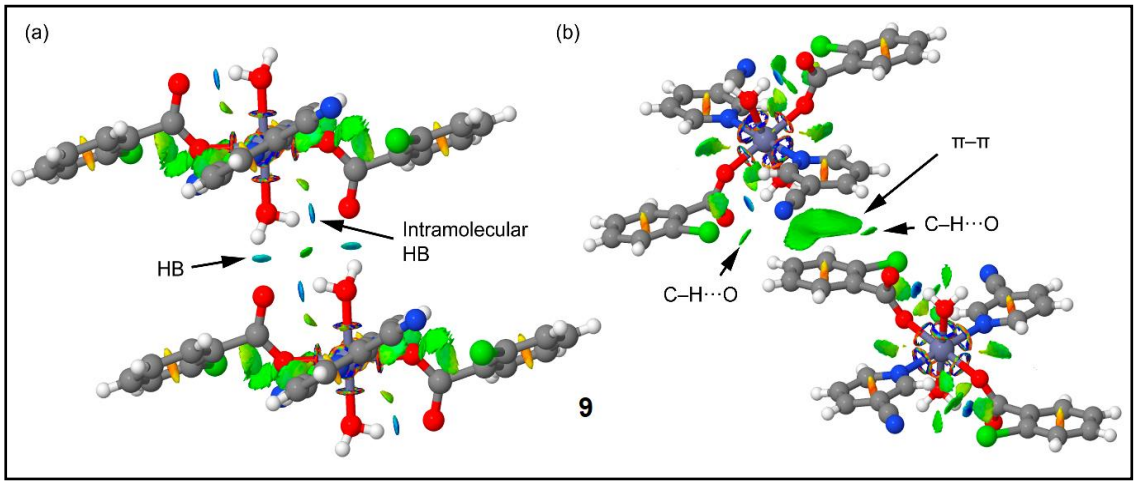

Figure 4.17 (**a**,**b**) NCI plots of the of the H-bonding and π–π dimers of compound **9**. The gradient cut-off is s = 0.35 a.u., and the colour scale is $-0.04 < \rho < 0.04$ a.u.

4.3.7 Thermal studies

Thermogravimetric analyses of complexes **7**, **8** and **9** were carried in the temperature range of 30-600°C under N_2 atmosphere at the heating rate of 10°C/min (**Figure 4.18**). In complex **7**, the first weight loss of 5.36% up to 116°C corresponds to

the loss of two coordinated aqua molecules (calculated = 5.86%).[67] In complexes **8** and **9**, the observed weight loss of 2.51% and 2.92% can be attributed to the loss of the first coordinated aqua molecule at temperature around 65°C (calculated = 2.95% and 2.90% respectively). This is in good agreement with strong coordination of the aqua ligand to cobalt(II) metal ion in **7** with shorter Co···O (water) bond distance than that in **8** and **9**.[68] Afterwards, for **7**, the mass loss of 53.77% in the temperature range of 118-388°C is attributed to the release of two *2-ClBz* moities (calculated = 50.64%).[69] Then it continues to degrade up to 600°C due to the loss of 1.5 molecules of *3-CNpy* (observed = 23.70%, calculated = 25.43%).[70] Recently, M. Heine *et al*. have also reported similar fractional weight loss of *3-CNpy* in the complex $[MnCl_2(3\text{-}CNpy)_2]_n$.[71]

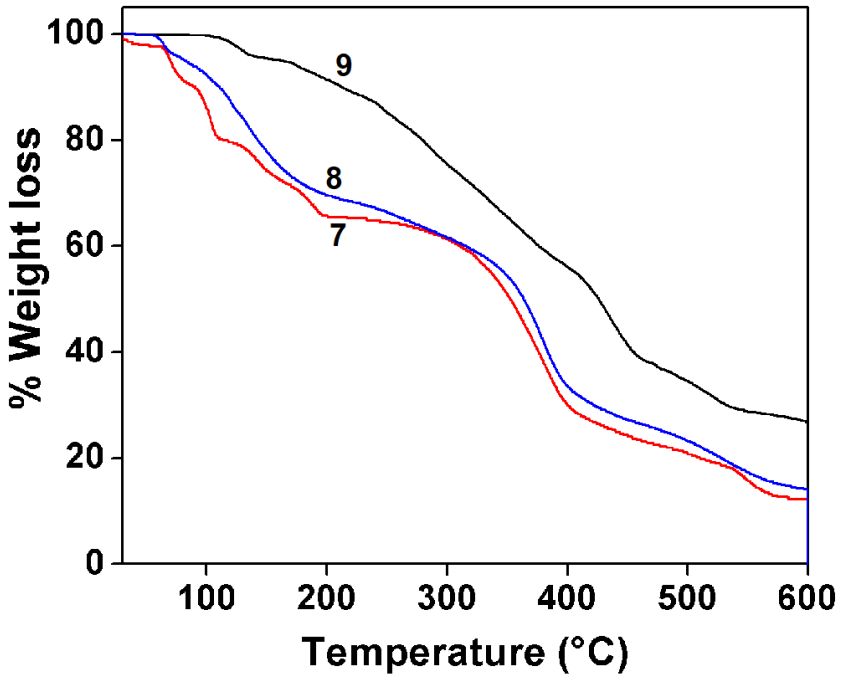

Figure 4.18 Thermogravimetric curves showing the thermal decomposition of complexes **7**, **8** and **9**.

For complex **8**, the second weight loss of 16.20% (calculated = 15.70%) in the temperature range of 68-106°C can be assigned to the release of the other coordinated aqua molecule along with 0.5 molecules of *2-ClBz* moiety. It further undergoes mass loss of 14.75% between 110 and 192°C, attributable to the loss of other 0.5 molecule of *2-ClBz* (calculated = 12.75%). It keeps losing weight up to 600°C, corresponding to the

loss of one *2-ClBz* and two *3-CNpy* moieties (observed = 57.66%, calculated = 59.61%). The complex **9** loses 26.65% of mass in the temperature range of 70-190°C, which can be assigned to the release of the other coordinated aqua molecule along with one *2-ClBz* molecule (calculated = 27.96%). Up to 600°C, it then loses the other *2-ClBz* along with the two *3-CNpy* (observed = 56.26%, calculated = 58.60%).[72]

4.3.8 MTT cell viability assay

The cytotoxic effects of the complexes **7**, **8** and **9** on DL and normal (PBMC) cells were evaluated by using MTT assay. MTT assays are considered to be important for the development of new drugs and also one of the most important preliminary screening methods for natural and synthetic compounds for studying cell proliferation and anticancer activities.[73] The analyses of cell viability results obtained for the compounds **7**, **8** and **9** on DL cell line treated for 24 hours showed significant concentration dependent decrease in cell viability (~ 25-30%) (**Figure 4.19**). Cell cytotoxicity was obtained for all the three compounds at the dose ranging from 1-10 μM within 24 hours. At the same time, negligible cytotoxic effect (~10%) was observed against normal PBMC cells as compared to cancer cell (DL).

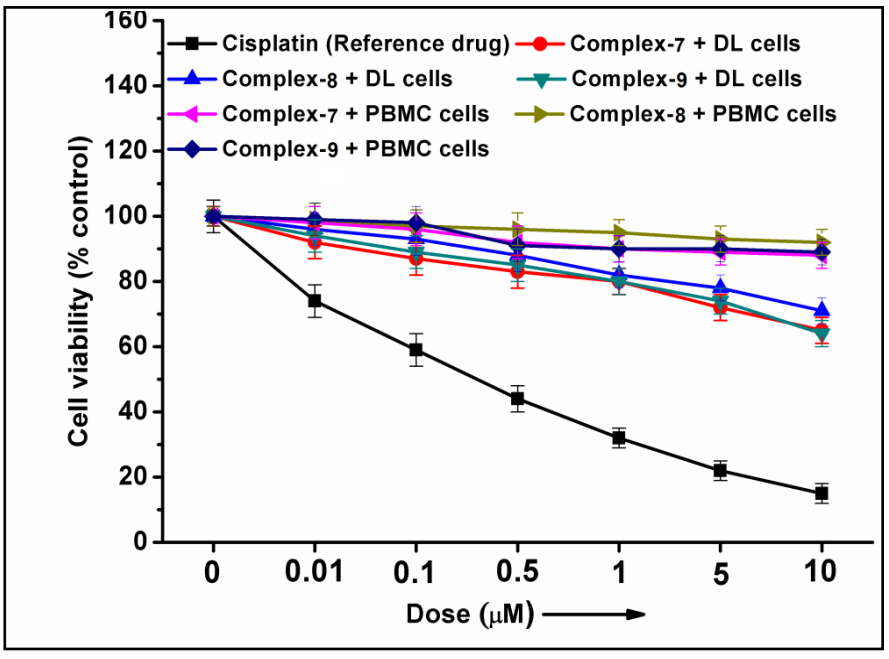

Figure 4.19 Cell viability study on DL and PBMC cells after treatment with the complexes **7**, **8** and **9** along with reference drug cisplatin at different dosage (0.01-10 μM) for 24 hours. Data are mean ±S.D., n = 3.

4.3.9 Cell proliferation and apoptosis assay

Apoptosis is a physiological process of cell death characterized by morphological features and mainly associated with severe DNA damage; the frequency and time of appearance of which depend on the cell line and the apoptosis-inducing signal.[74] In order to investigate the action of the complexes on morphological changes in DL cells, acridine orange (AO)/ethidium bromide (EB) dual staining method was used under fluorescence microscopy. AO is a crucial dye that can stain nuclear DNA of viable cells with intact cell membrane and uniformly stained green while EB can only stain cells that had lost their membrane integrity[75] and appears red or orange. The results of apoptotic study in control group showed mostly viable DL cells identified by bright uniform green nuclei (**Figure 4.20**).

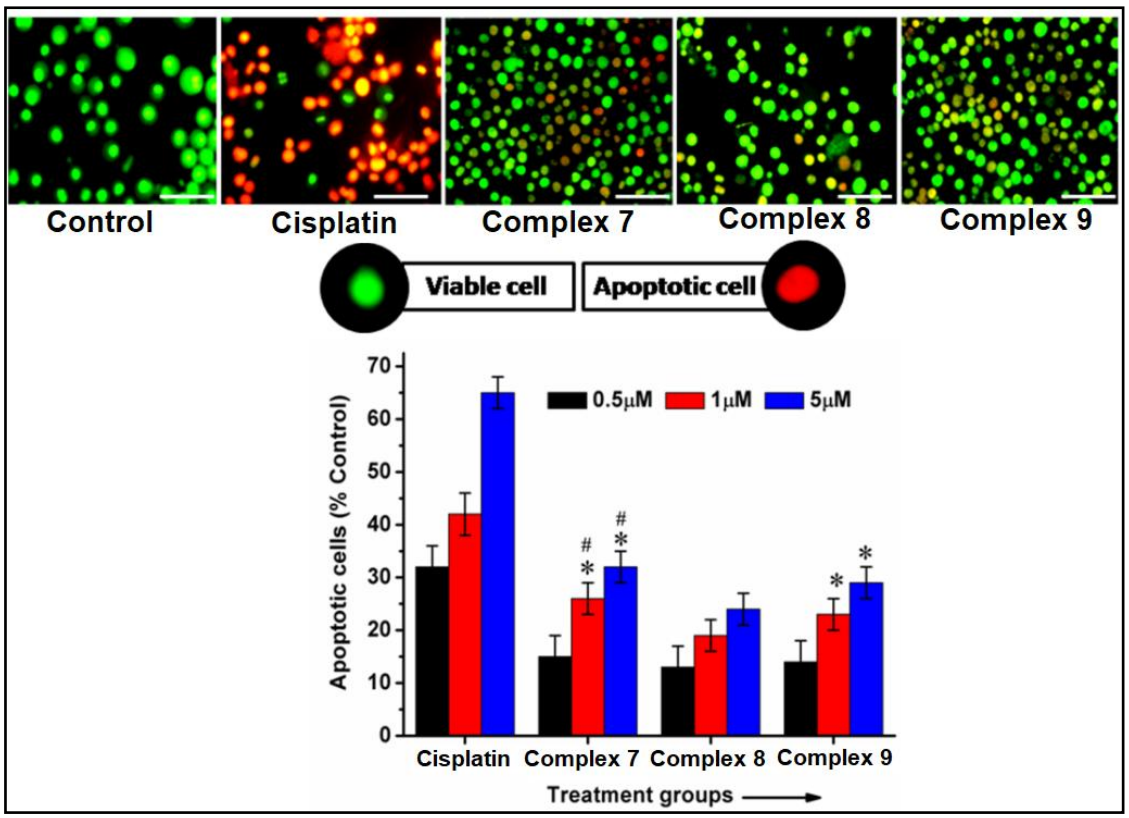

Figure 4.20 Upper panel showed morphological features of apoptotic and viable cells. Control DL cells showed mostly viable cells, cisplatin and complexes **7**, **8** and **9** treated groups showing apoptotic features evident by red/orange nuclei with membrane damage and blebbing. Scale bar 50 μm. Lower panel showed percentage apoptotic cells after treatment with complexes and the reference drug, cisplatin at different dosage. Data are mean ± S.D., n = 3, ANOVA, $P \leq 0.05$. ANOVA significance symbol: * with respect to complex **8** and # with respect to complex **9**.

Complexes **7**, **8** and **9** treated cells showed concentration-dependent increase in apoptotic features in DL cells. Lower concentration such as 0.5 μM showed mostly early apoptotic cells with nuclear marginalization and chromatin condensation. Whereas higher concentrations (1 and 5 μM) showed late apoptotic features which include fragmented chromatin, cytoplasmic vacuoles and apoptotic bodies. The results suggested that all the three complexes were able to induce apoptosis in DL cells. Moreover, it can be seen that cisplatin induced more apoptotic cell death against DL cells than that of the complexes. It has been reported that pyridine derivatives induce cancer cell apoptosis by triggering DNA damage-mediated p53 phosphorylation (tumor suppressor) in A375 malignent melanoma cell lines.[76] Ruthenium pyridyl complexes have also been demonstrated potent antiproliferative activity, and induce mitochondria-mediated and caspase-dependent apoptosis in human cancer cells through regulation of BCL-2 family members and activation of caspases.[77]

4.3.10 Molecular docking studies

The *in silico* docking technique can be exploited to build targets and design inhibitors for novel therapeutic agents. Molecular docking helps in understanding the action of neoplastic drugs (*chemotherapeutic drugs used to treat cancer*) through affinity binding. A number of studies have recently shed light onto the role of pro- and anti-apoptotic BCL-2 protein family members in tumor-pathogenesis and in mediating the effects of classical as well as novel front-line anticancer agents, allowing the development of more efficient and more precisely targeted treatment regimens.[78] In the present study, molecular docking simulation has been used to dissect possible mechanism of action of complexes **7**, **8** and **9** associated with cytotoxicity and apoptosis due to their interactions with anti-apoptotic proteins (BCL-2). Anti-apoptotic BCL-2 proteins play a major role in tumor cell survival and are closely associated with various stages of cell multiplication and hence responsible for the propagation of cancer.[79] by inhibiting apoptosis. BCL-2 inhibitors have been developed as direct inducers of apoptosis and their inhibition by various chemotherapeutic agents is associated with the apoptotic induction that inhibits the cancer growth and invasion.[80] Docking was validated by redocking the original ligands present in the active sites of receptor as observed in crystallographic pdb file (PDB ID: 2O22).

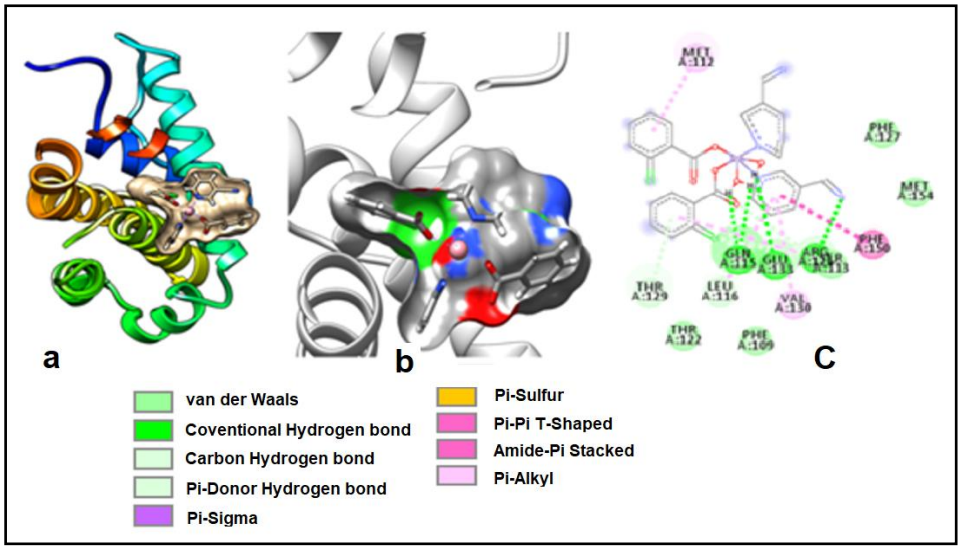

Figure 4.21 Docking structure of complex $[Co(3\text{-}CNpy)_2(2\text{-}ClBz)_2(H_2O)_2]$ (**7**) with BCL-2 receptor. Chemical interactions are shown in dotted lines along with ligand atoms labeling and interacting amino acids in the inhibitors binding sites of BCL-2 receptor; (**a**) Docked pose of receptor-compound complex in ribbon view; (**b**) surface view of active sites with the complex **7**; (**c**) interacting residues are shown in receptor active sites.

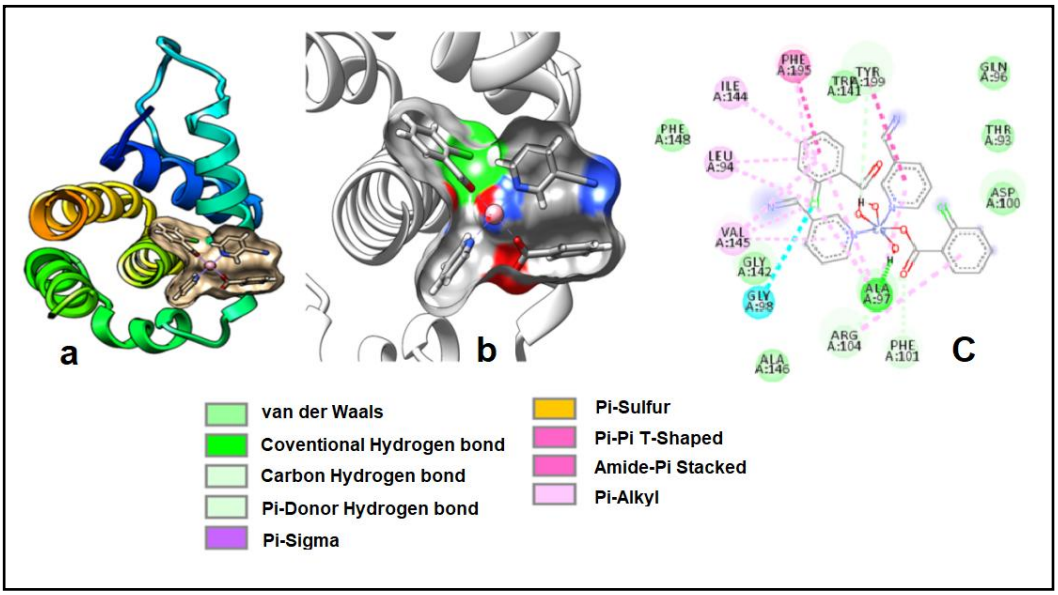

Figure 4.22 Docking structure of complex $[Mn(3\text{-}CNpy)_2(2\text{-}ClBz)_2(H_2O)_2]$ (**8**) with BCL-2 receptor. Chemical interactions are shown in dotted lines along with ligand atoms labeling and interacting amino acids in the inhibitors binding sites of BCL-2 receptor; (**a**) Docked pose of receptor-compound complex in ribbon view; (**b**) surface view of active sites with the complex **8**; (**c**) interacting residues are shown in receptor active sites.

The molecular docking studies revealed that the compounds are promising, which is supported by their low binding energy (high affinity for receptor) and strong hydrogen bonding interactions with the exposed active site amino acids of target protein BCL-2 which may cause cytotoxicity and induce apoptosis in cancer cells. The interactions of the active site amino acids of BCL-2 with the compounds **7**, **8** and **9** are shown in **Figures 4.21-4.23**. These interactions play important roles for the stability of the target-compound complexes. The MVD (Molegro Virtual Docker) docking score of the complexes **7**, **8** and **9** are shown in **Figure 4.24**. Thus, based on the docking analysis, all the compounds indicated potential apoptotic inducing ability due to their efficient interaction with anti-apoptotic target proteins.

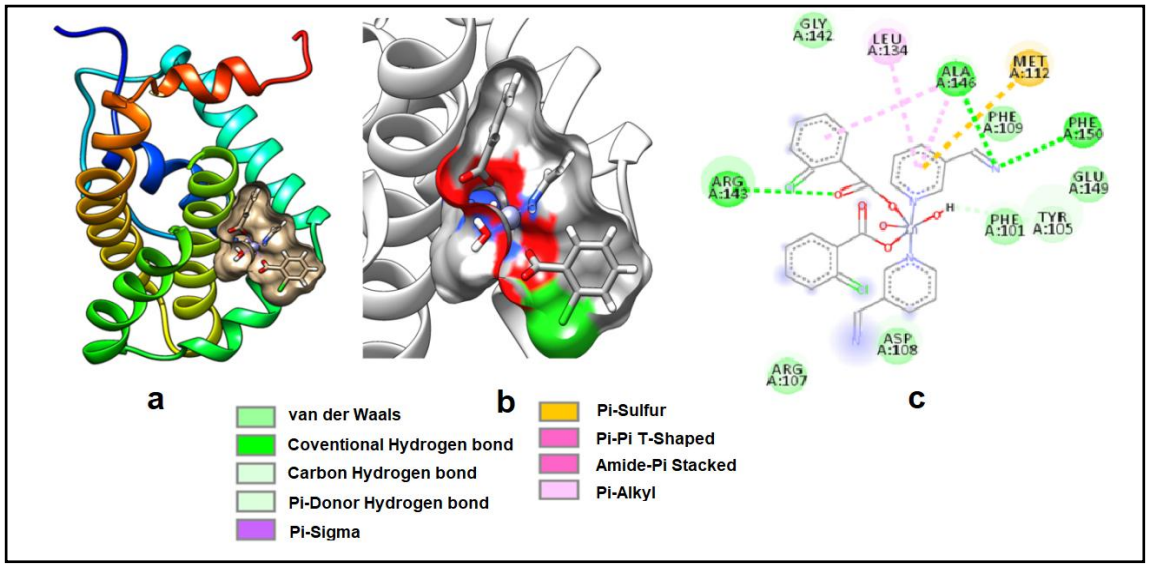

Figure 4.23 Docking structure of complex $[Zn(3\text{-}CNpy)_2(2\text{-}ClBz)_2(H_2O)_2]$ (**9**) with BCL-2 receptor. Chemical interactions are shown in dotted lines along with ligand atoms labeling and interacting amino acids in the inhibitors binding sites of BCL-2 receptor (**a**) Docked pose of receptor-compound complex in ribbon view (**b**) surface view of active sites with complex **9** (**c**) interacting residues are shown in receptor active sites.

4.3.11 Pharmacophore modelling

In modern computational and medicinal chemistry, pharmacophore features are useful to identify the essential components of one or multiple molecules with similar biological activities.[81] Ligandscout automatically derives key chemical features, such as hydrogen bond donors and acceptors, hydrophobic, positive and negative ionizable,

aromatic interactions along with their 3D geometries of bioactive molecules. Pharmacophore features also represent signature of chemical compounds which can be used to search for more molecules with known biological activities based on same chemical group(s) arranged in the same 3D orientation. To be effective as a drug candidate, a bioactive compound(s) must reach its target destination and stay in the body without losing potency for the expected biological events to occur. In that context, computer models constitute valid alternatives to experiments. Here, we have identified important pharmacophore features of the synthesized compounds such as hydrophobic, aromatic, positive ionizable, negative ionizable, H-bond donor, H-bond acceptor and halogen bond donor that may be responsible for biological activities (**Figure 4.25**).

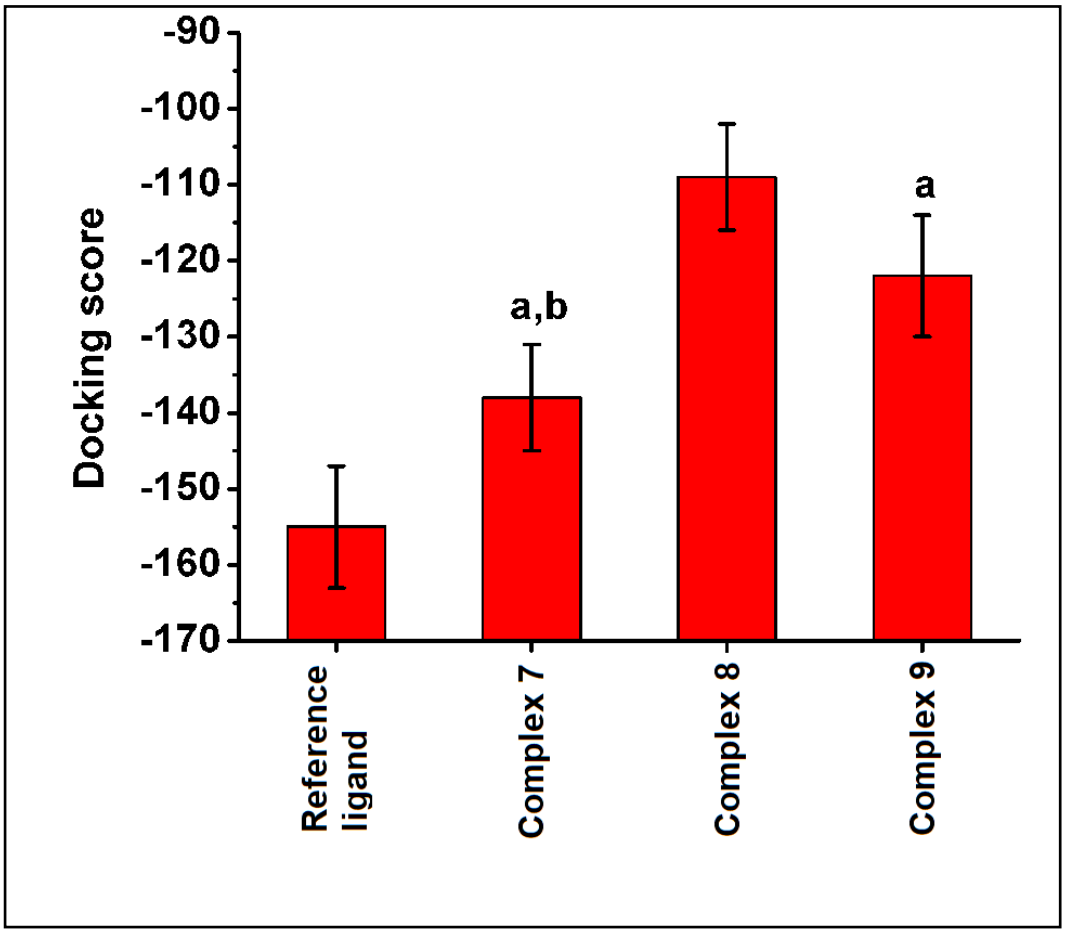

Figure 4.24 Docking scores of complexes **7**, **8** and **9** with BCL-2 receptors. As per MVD docking score algorithm, lowest the score better is the interactions. Data are mean ± S.D, n = 3, ANOVA, $P \leq 0.05$. ANOVA significance symbol: (**a**) with respect to complex **8** and (**b**) with respect to complex **9**.

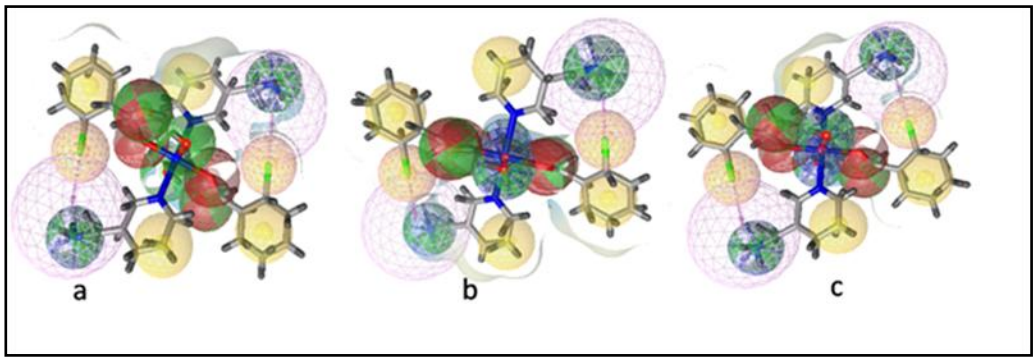

Figure 4.25 Pharmacophore features of complex (**a**) $[Co(3\text{-}CNpy)_2(2\text{-}ClBz)_2(H_2O)_2]$ (**7**), (**b**) $[Mn(3\text{-}CNpy)_2(2\text{-}ClBz)_2(H_2O)_2]$ (**8**) and (**c**) $[Zn(3\text{-}CNpy)_2(2\text{-}ClBz)_2(H_2O)_2]$ (**9**) responsible for biological activities. Pharmacophore feature including hydrophobic, positive ionizable, negative ionizable, acceptor and halogen bond donor interactions are depicted as yellow spheres, blue star, red star, red arrows and excluded volume, respectively.

4.4 CONCLUSIONS

Three new isostructural complexes of Co(II), Mn(II) and Zn(II) *viz*. $[Co(3\text{-}CNpy)_2(2\text{-}ClBz)_2(H_2O)_2]$ (**7**), $[Mn(3\text{-}CNpy)_2(2\text{-}ClBz)_2(H_2O)_2]$ (**8**) and $[Zn(3\text{-}CNpy)_2(2\text{-}ClBz)_2(H_2O)_2]$ (**9**) have been synthesized and characterized by single crystal X-ray diffraction, electronic, vibrational, PXRD and TGA analyses. Furthermore, using Fabian and Kalman approach, their isostructurality parameters have been evaluated. Electrostatically enhanced π-π stacking interactions are observed between the coordinated *3-CNpy* (π-acidic) of one complex unit and the phenyl moiety of *2-ClBz* (π-basic) from a neighbouring monomeric unit. These interactions along with relevant H-bonding have been investigated by molecular DFT calculations, MEP surfaces and characterized using the NCI plot index analysis. The study reveals that the H-bonded assembly is more favorable than the π-stacking interactions. However, the π-stacking energy is electrostatically enhanced and is stronger than usual staking interactions involving arenes with negligible influence of the metal centers. All the three complexes significantly inhibit cell viability by inducing apoptotic cell death in DL malignant cancer cells with negligible cytotoxicity in normal cells. The *in silico* molecular docking study reveals that the complexes **7**, **8** and **9** interact and accommodated well in the active site of anti-apoptotic protein BCL-2 that lead to apoptotic cell death. Furthermore, the pharmacophore features such as hydrophobic, aromatic, positive

ionizable, negative ionizable, H-bond donor, H-bond acceptor and halogen bond donor of the complexes may play important role for their biological activities based on structure activity relationship (SAR).

REFERENCES

1. (a) Bishop, M. M.; Coles, S. J.; Andrew, H. W. L.; Linndoy, L. F.; Parkin, A.; Thorn-Seshold, O. T.; Turner, P. *Supramol. Chem*. **2005**, *17*, 567.

(b) Zhou, L. J.; Wang, Y. Y.; Zhou, C. H; Wang, C. J; Shi, Q. Z.; Peng, S. M. *Cryst. Growth Des.* **2007**, *7*, 300.

(c) Diaz, P.; Benet-Buchholz, J.; Vilar, R.; White, A. J. P. *Inorg. Chem*. **2006**, *45*, 1617.

(d) Bhattacharyya, M. K.; Saha, U.; Dutta, D.; Das, A.; Verma, A. K.; Frontera, A. *RSC Adv*. **2019**, *9*, 16339.

(e) Miras, H. N.; Sorus, M.; Hawkett, J.; Sells, D. O.; McInnes, E. J. L.; Cronin, L. *J. Am. Chem. Soc.* **2012**, *134*, 6980.

2. (a) Khavasi, H. R.; Sadegh, B. M. M. *Inorg. Chem*. **2010**, *49*, 5356.

(b) Jung, O. S.; Park, S. H.; Kim, K. M.; Jang, H. G. *Inorg. Chem*. **1998**, *37*, 5781.

(c) Ovejero, P.; Mayoral, M. J.; Cano, M.; Campo, J. A.; Heras, J. V.; Pinilla, E.; Torres, M. R. *J. Organomet. Chem*. **2007**, *692*, 4093.

(d) Karrouchi, K.; Yousfi, E. B.; Sebbar, N. K.; Ramli, Y.; Taoufik, J.; Ouzidan, Y.; Ansar, M.; Mabkhot, Y. N.; Ghabbour, H. A.; Radi, S. *Int. J. Mol. Sci.* **2017**, *18*, 2215.

3. (a) Mirzaei, M.; Eshtiagh-Hosseini, H.; Bolouri, Z.; Rahmati, Z.; Esmaeilzadeh, A.; Hassanpoor, A.; Bauza, A.; Ballester, P.; Barcelo´-Oliver, M.; Mague, J. T.; Notash, B. Frontera, A. *Cryst. Growth Des*. **2015**, *15*, 1351.

(b) Carlucci, L.; Ciani, G.; Proserpio, D. M.; Rizzato, S. *Chem. Eur. J.* **1999**, *5*, 237.

(c) Ma, J. F.; Liu, J. F.; Yan, X.; Jia, H. Q.; Lin, Y. H. *Dalton Trans*. **2000**, 2403.

(d) Aakeröy, C. B.; Champness, N. R.; Janiak, C. *CrystEngComm*. **2010**, *12*, 22.

4. (a) Ye, B. H.; Tong, M. L.; Chen, X. M. *Coord. Chem. Rev*. **2005**, *249*, 545.

(b) Dutta, D.; Nath, H.; Frontera, A.; Bhattacharyya, M. K. *Inorg. Chim. Acta* **2019**, *487*, 354.

5. (a) Biswas, C.; Mukherjee, P.; Drew, M. G. B.; Gomez-Garcia, C. J.; Clemente-Juan, J. M.; Ghosh, A. *Inorg. Chem*. **2007**, *46*, 10771.

(b) Baruah, A. M.; Karmakar, A.; Baruah, J. B. *Inorg. Chim. Acta* **2008**, *361*, 2777.

(c) Hazra, S.; Sarkar, B.; Naiya, S.; Drew, M. G. B.; Frontera, A.; Escudero, D.; Ghosh, A. *Cryst. Growth Des*. **2010**, *10*, 1677.

(d) Ray, M. S.; Ghosh, A.; Das, A.; Drew, M. G. B; Ribas-Arino, J.; Novoa, J.; Ribas, J. *Chem. Commun.* **2004**, 1102.

6. (a) Liu, F. Q.; Wang, Q. X.; Jiao, K.; Jian, F. F.; Liu, G. Y.; Li, R. X. *Inorg. Chim. Acta* **2006**, *359*, 1524.

(b) Moncol, J.; Korabik, M.; Segla, P.; Koman, M.; Miklos, D.; Jaskova, J.; Glowiak, T.; Melnık, M.; Mrozinski, J.; Sundberg, M. R. *Z. Anorg. Allg. Chem*. **2007**, *633*, 298.

7. Adonin, S. A.; Petrov, M. D.; Novikov, A. S.; Shiriyazdanov, R. R.; Sokolov, M. N.; Fedin, V.P. *J. Clust. Sci*. **2019**, *30*, 857.

8. Barcelo-Oliver, M.; Garcia-Raso, A.; Terron, A.; Molins, E; Prieto, M. J.; Moreno, V.; Martınez, J.; Llado, V.; Lopez, I.; Gutierrez, A;, Escriba, P. V. *J. Inorg. Biochem*. **2007**, *101*, 649.

9. (a) Deng, D.; Liu, P.; Fu, W.; Li, L.; Yang, F.; Ji, B. *Inorg. Chim. Acta* **2010**, *363*, 891.

(b) MacDonald, J. C.; Dorrestein, P. C.; Pilley, M. M.; Foote, M. M.; Lundburg, J. L.; Henning, R. W.; Schultz, A. J.; Manson, J. L. *J. Am. Chem. Soc.* **2000**, *122*, 11692.

10. Saysell, C. G.; Borman, C. D.; Baron, A. J.; McPherson, M. J.; Sykes, A. G. *Inorg. Chem.* **1997**, *36*, 4520.

11. Yang, L.; Crans, D. C.; Miller, S. M.; Cour, A.; Anderson, O. P.; Kaszynski, P. M.; Godzala, M. E.; Austin, L. T. D.; Willsky, G. R. *Inorg. Chem.* **2002**, *41*, 4859.

12. (a) Scapin, G.; Reddy, S. G.; Zheng, R.; Blanchard, J. S. *Biochemistry* **1997**, *36*, 15081.

(b) Martin, B. L. *Arch. Biochem. Biophys.* **1997**, *345*, 332.

13. Hegde, D.; Dodamani, S.; Kumbar, V.; Jalalpure, S.; Gudasi, K. *Appl. Organometal Chem.* **2017**, *31*, 3851.

14. (a) Gogoi, A.; Islam, S. M. N.; Frontera, A.; Bhattacharyya, M. K. *Inorg. Chim. Acta* **2019**, *484*, 133.

(b) Dinolfo, P. H.; Benkstein, K. D.; Stern, C. L.; Hupp, J. T. *Inorg. Chem*. **2005**, *44*, 8707.

(c) Noro, S.; Kitagawa, S.; Nakamura, T.; Wada, T. *Inorg. Chem*. **2005**, *44*, 3960.

15. (a) Sikorski, A.; Trzybiński, D. *J. Mol. Struct*. **2013**, *1049*, 90.

(b) Bauza, A.; Mooibroek, T. J.; Frontera, A. *Chem. Phys. Chem.* **2015**, *16*, 2496.

16. (a) Kitagawa, S.; Noro, S. *Comprehensive Coordination Chemistry II* **2004**, *7*, 231.

(b) Constable, E. C.; Dunphy, E. L.; Housecroft, C. E.; Neuburger, M.; Schaffner, S.; Schapera, F.; Batten, S. R. *Dalton Trans*. **2007**, 4323.

17. Su, F.; Lu, L.; Feng, S.; Zhu, M.; Gao, Z.; Dong, Y.; *Dalton Trans*. **2007**, 4323.

18. Wen, L.; Wang, D.; Chen, Y.; Meng, X.; Li, D.; Lan, S. *J. Coord. Chem*. **2009**, *62*, 789.

19. Guan, Q.; Shi, X.; Shen, J.; Zhao, G. *Sci. China Chem*. **2013**, *56*, 588.

20. (a) Garau, C.; Quinonero, D; Frontera, A.; Ballester, P.; Costa, A.; Deya, P. M. *J. Phys. Chem.* **2005**, *109*, 9341.

(b) Quinonero, D.; Frontera, A.; Garau, C.; Ballester, P.; Costa, A.; Deya, P. M. *Chem. Phys. Chem.* **2006**, *7*, 2487.

(c) Frontera, A.; Quinonero, D.; Costa, A.; Ballester, P.; Deya, P. M. *New J. Chem.* **2007**, *31*, 556.

(d) Garcıa-Raso, A.; Albertı, F. M.; Fiol, J. J.; Tasada, A.; Barcelo-Oliver, M.; Molins, E.; Escudero, D.; Frontera, A.; Quinonero, D.; Deya, P. M. *Inorg. Chem.* **2007**, *46*, 10724.

(e) Barrios, L. A.; Aromi, G.; Frontera, A.; Quinonero, D.; Deya, P. M.; Gamez, P.; Roubeau, O.; Shotton, E. J.; Teat, S. J. *Inorg. Chem.* **2008**, *47*, 5873.

21. (a) Metrangolo, P.; Resnati, G. *Chem. Eur. J*. **2001**, *7*, 2511.

(b) Alkorta, I.; Blanco, F.; Deyà, P. M.; Elguero, J.; Estarellas, C.; Frontera, A.; Quiñonero, D. *Theor. Chem. Acc.* **2010**, *126*, 1.

22. Bauzá, A.; Frontera, A. *Phys. Chem. Chem. Phys.* **2016**, *18*, 20381.

23. (a) Amabilino, D. B.; Stoddart, J. F. *Chem. Rev.* **1995**, *95*, 2725.

(b) Claessens, C. G.; Stoddart, J. F. *J. Phys. Org. Chem.* **1997**, *10*, 254.

(c) Hirsch, K. A.; Wilson, S. R.; Moore, J. S. *Chem. Eur. J*. **1997**, *3*, 765.

24. (a) Lightfoot, M. P.; Mair, F. S.; Pritchard, R. G.; Warren, J. W. *Chem. Commun*. **1999**, 1945.

(b) Ning, G. L.; Wu, L. P.; Sugimoto, K.; Munakata, M.; Kuroda-Sowa, T.; Maekawa, M. *Dalton Trans*. **1999**, 2529.

(c) Brown, S. P.; Schnell, I.; Brand, J. D.; Müllen, K.; Spiess, H. W. *J. Am. Chem. Soc*. **1999**, *121*, 6712.

(d) Lamsa, M.; Huuskonen, J.; Rissanen, K.; Pursiainen, J. *Chem. Eur. J*. **1998**, *4*, 84.

25. (a) Rappe, A. K.; Bernstein, E. R. J. *J. Phys. Chem. A* **2000**, *104*, 6117.

(b) Hesselmann, A.; Jansen, G.; Schutz, M. J. *J. Am. Chem. Soc*. **2006**, *128*, 11730.

26. Sheldrick, G. M. *Acta Crystallogr. Sect: A* **2008**, *64*, 11.

27. Brandenburg, K. *Diamond 3.1f, Crystal Impact GbR*, Bonn, Germany **2008**

28. Frisch, M. J.; Trucks, G. W.; Schlegel, H. B.; Scuseria, G. E.; Robb, M. A.; Cheeseman, J. R.; Scalmani, G.; Barone, V.; Mennucci, B.; Petersson, G. A.; Nakatsuji, H.; Caricato, M.; Li X.; Hratchian, H. P.; Izmaylov, A.F.; Bloino, J.; Zheng, G.; Sonnenberg, J. L.; Hada, M.; Ehara, M.; Toyota, K.; Fukuda, R.; Hasegawa, J.; Ishida, M.; Nakajima, T.; Honda, Y.; Kitao, O.; Nakai, H.; Vreven, T.; Montgomery Jr., J. A.; Peralta, J. E.; Ogliaro, F.; Bearpark, M.; Heyd, J. J.; Brothers, E.; Kudin, K. N.; Staroverov, V. N.; Kobayashi, R.; Normand, J.; Raghavachari, K.; Rendell, A.; Burant, J. C.; Iyengar, S. S.; Tomasi, J.; Cossi, M.; Rega, N.; Millam, J. M.; Klene, M.; Knox, J. E.; Cross, J. B.; Bakken, V.; Adamo, C.; Jaramillo, J.; Gomperts, R.; Stratmann, R. E.; Yazyev, O.; Austin, A. J.; Cammi, R.; Pomelli, C.; Ochterski, J. W.; Martin, R. L.; Morokuma, K.; Zakrzewski, V. G.; Voth, G. A.; Salvador, P.; Dannenberg, J. J.; Dapprich, S.; Daniels, A. D.; Farkas, O.; Foresman, J. B.; Ortiz, J. V.; Cioslowski, J.; Fox, D. J. Gaussian 09, Gaussian Inc., Wallingford C. T. **2009.**

29. Grimme, S.; Antony, J.; Ehrlich, S.; Krieg, H. *J. Chem. Phys*. **2010**, *132*, 154104.

30. Boys, S. F.; Bernardi, F. *Mol. Phys*. **1970**, *19*, 553.

31. Contreras-Garcia, J.; Johnson, E. R.; Keinan, S.; Chaudret, R.; Piquemal, J. P.; Beratan, D. N.; Yang, W. *J. Chem. Theory Comput*. **2011**, *7*, 625.

32. Mosmann, T. *J. Immunol. Methods* **1983**, *16*, 55.

33. Verma, A. K.; Prasad S. B. *Anticancer Agents Med. Chem.* **2013**, *13*, 1096.

34. Squier, M. K.; Cohen, J. J. *Mol. Biotechnol.* **2001**, *19*, 305.

35. Prasad, S. B.; Verma, A. K. *Microsc. Microanal.* **2013**, *19*, 1377.

36. Frenzel, A.; Grepsi, F.; Chmelewskij, W.; Villunger, A. *Apoptosis* **2009**, *14*, 584.

37. Yip, K. W.; Reed, J. C. *Oncogene* **2008**, *27*, 6398.

38. Soderquist, R. S.; Eastman, A. *Mol. Cancer Ther*. **2016**, *15*, 2011.

39. Al-Shaer, M. A.; Al-Balas, Q. A.; Hassan, M. A.; Al Jabal, G. A.; Almaaytah, A. M. *Comput. Biol. Chem.* ***2019***, *80*, 102.

40. (a) Banerjee, A.; Chattopadhyay, S. *Polyhedron* **2020**, *177*, 114290.

(b) Hamil, A.; Khalifa, K. M.; Almutaleb, A. A.; Qasim, M.; *Adv. J. Chem*. **2020**, *3*, 524.

41. Nakamoto, K. *Infrared and Raman Spectra of Inorganic and Coordination Compounds, fifth ed*., John Wiley & Sons, New York **1997**.

42. Saha, U.; Dutta, D.; Nath, H.; Franconetti, A.; Frontera, A.; Bhattacharyya, M. K. *Inorg. Chim. Acta* **2019**, *488*, 159.

43. Tao, J.; Tong, M. L.; Chen, X. M. *Dalton Trans*. **2000**, 3669.

44. Farkas, B.; Terranova, U.; Leeuw, N. *Phys. Chem. Chem*. *Phys*. **2020**, *22*, 985.

45. Heine, M.; Fink, L.; Schmidt, M. U. *CrystEngComm*. **2019**, *21*, 4305.

46. Wang, S. P.; Zhou, J. J.; Zhao, S. Y.; Zhao, Y.; Ma, X. B. *Chin. Chem. Lett*. **2015**, *26*, 1096.

47. Bora, S. J.; Das, B. K. *J. Solid State Chem*. **2012**, *192*, 93.

48. Ghosh, M.; Majee, A.; Nethaji, M.; Chattopadhyay, T. *Inorg. Chim. Acta* **2009**, *362*, 2052.

49. Singh, K.; Kumar, Y.; Puri, P.; Sharma, C.; Aneja, K. R. *Arab. J. Chem*. **2017**, *10*, 978.

50. (a) Lever, A. B. P. *Inorganic Electronic Spectroscopy*, second ed., Elsevier Science, Amsterdam, **1984**.

(b) Asada, H.; Hayashi, K.; Negoro, S.; Fujiwara, M.; Matsushita, T. *Inorg. Chem. Commun.* **2003**, *6*, 193.

51. (a) Basumatary, D.; Lal, R. A.; Kumar, A. *J. Mol. Struct*. **2015**, *1092*, 122.

(b) Chu, Z.; Huang, W. *Inorg. Chem. Commun*. **2008**, *11*, 1166.

52. Zhang, C. S.; Li, J.; Hou, K. L.; Xing, Y. H.; Shi, Z. *Spectrochim. Acta* **2011**, *78*, 777.

53. (a) Aligo, J. A.; Smith, L.; Eglin, J. L.; Pence, L. E. *Inorg. Chem*. **2005**, *44*, 4001.

(b) Dutta, D.; Islam, S. M. N.; Saha, U.; Chetry, S.; Guha, A. K.; Bhattacharyya, M. K. *J. Chem. Crystallogr*. **2018**, *48*, 156.

(c) Hegde, D.; Dodamani, S.; Kumbar, V.; Jalalpure, S.; Gudasi, K. B. *Appl. Organometal. Chem.* **2017**, 3851.

54. Kumar, B.; Kumar, S.; Kumar, D.; Sharma, S. *Orient. J. Chem*. **2017**, *33*, 2643.

55. Yenikaya, C.; Poyraz, M.; Sari, M.; Demirci, F.; Ilkimen, H.; Buyukgungor, O. *Polyhedron* **2009**, *28*, 3526.

56. (a) Xu, T. G.; Xu, D. J. *Acta Crystallogr. Sect. E* **2004**, *60*, 1131.

(b) Hokelek, T.; Necefoglu, H. *Acta Crystallogr. Sect. C* **1998**, *54*, 1242.

(c) Beattie, J. K.; Hambley, T. W.; Klepetko, J. A.; Masters, A. F.; Turners, P. *Polyhedron* **1996**, *15*, 473.

(d) Islam, S. M. N.; Dutta, D.; Verma, A. K.; Nath, H.; Frontera, A.; Sharma, P.; Bhattacharyya, M. K. *Inorg. Chim. Acta* **2019**, *498*, 119161.

57. Stefanou, V.; Matiadis, D.; Tsironis, D.; Igglessi-Markopoulou, O.; McKee, V. *J. Markopoulos* **2018**, *141*, 289.

58. Tocana, E.; Siminel, A.; Croitor, L. *Chem. J. Mol.* **2017**, *12*, 102.

59. Stephenson, M. D.; Hardie, M. J. *Cryst. Growth Des.* **2006**, 6, 423.

60. Hokelek, T.; Akduran, N.; Ozen, A.; Ugurluc, G.; Necefoglu, H. *Acta Cryst.* **2017**, *73*, 413.

61. Etter, M. C. *Acc. Chem. Res.* **1990**, *23*, 120.

62. Moro, A. C.; Watanabe, F. W.; Ananias, S. R.; Mauro, A. E.; Netto, A. V. G.; Lim, A. P. R.; Ferreir, J. G.; Santos, R. H. A. *Inorg. Chem. Commun*. **2006**, *9*, 493.

63. Fábián, L.; Kálmán, A., *Acta Cryst*. **1999**, *B55*, 1099.

64. Das, B. K.; Bora, S. J.; Bhattacharyya, M. K.; Barman, R. K. *Acta Cryst*. **2009**, *B65*, 467.

65. Croitor, L.; Chisca, D.; Coropceanu, E. B.; Volodina, G. F.; Petuhov, O.; Fonari, M. S. *J. Mol. Struct*. **2017**, *1137*, 136.

66. Borah, S.; Kalita, A. C.; Gogoi, N. *Z. Anorg. Allg. Chem*. **2014**, *640*, 1789.

67. Huang, W.; Hu, D.; Gou, S.; Qian, H.; Fun, H. K.; Raj, S. S. S.; Meng, Q. *J. Mol. Struct*. **2003**, *649*, 269.

68. Li, D. Yang, D.; Zhu, X.; Jina, D.; Xia, Y.; Ji, Q.; Cai, R. *J. Mater. Chem. A* **2014**, *2*, 18761.

69. Hwang, I. H.; Jo, Y. D.; Kim, H. Y.; Kang, J.; Noh, J. Y.; Hyun, M. Y.; Kim, C.; Kim, Y.; Kim, S. J. *Polyhedron* **2012**, *42*, 282.

70. Sun, D.; Wei, Z. H.; Yang, C. F.; Wang, D. F.; Zhang, N.; Huang, R. B.; Zheng, L. S. *CrystEngComm.* **2011**, *13*, 1591.

71. Heine, M.; Fink, L.; Schmidt, M. U. *CrystEngComm.* **2019**, *21*, 4305.

72. (a) Tian, G.; Zhu, G.; Yang, X.; Fang, Q.; Xue, M.; Sun, J.; Wei, Y.; Qiu, S. *Chem. Commun.* **2005**, 1396

(b) Ahmad, T.; Ramanujachary, K. V.; Lofland, S. E.; Ganguli, A. K. *J. Mater. Chem* **2004**, *14*, 3406.

73. (a) Teixeira, R. R.; Barbosa, L. C.; Maltha, C. R. A.; Rocha, M. E.; Bezerra, D. P.; Costa-Lotuf, L. V.; Pessoa, C.; Moraes, M. O. *Molecules* **2007**, *12*, 1101.

(b) Jamalian, A.; Miri, R.; Firuzi, O.; Amini, M.; Moosavi-Movahedi, A.; Shafieea, A. *J. Iran. Chem. Soc.* **2011**, *8*, 983.

74. Wu, J.; Yi, W.; Jin, L.; Hu, D.; Song B. *Cell division* **2012**, *7*, 20.

75. Xu, X.; Gao, X.; Jin, L.; Bhadury, P. S.; Yuan, K.; Hu, D.; Song, B.; Yang, S. *Cell division* **2011**, *6*, 1.

76. Li, L.; Cao, W.; Zheng, W.; Fan, C.; Chen, T. *Dalton Trans*. **2012**, *41*, 12766.

77. Chen, T.; Liu, Y.; Zheng, W. J.; Liu, J.; Wong, Y. S. *Inorg. Chem*. **2010**, *49*, 6366.

78. Thomsen, R.; Christensen, M. H. *J. Med. Chem*. **2006**, *49(11)*, 3315

79. Bhattacharyya, M. K.; Gogoi, A.; Chetry, S.; Dutta, D.; Verma, A. K.; Sarma, B.; Franconetti, A.; Frontera, A. *J. Inorg. Biochem*. **2019**, *200*, 110803.

80. (a) Thomsen, R.; Christensen, M. H. *J. Med. Chem*. **2006**, *49*, 3315.

(b) Verma, A. K.; Prasad, S. B. *Anti-cancer Agent Med. Chem.* **2013**, *13*, 1096.

81. Wolber, G.; Langer, T. *J. Chem. Inf. Model* **2005**, *45*, 160.